# Chapter 2. An X-ray computed tomography study of inclusion trail orientations in multiple porphyroblasts from a single sample

# Abstract

Inclusion trails in 58 garnet porphyroblasts in a single sample from the Cram Hill Formation in southeast Vermont were imaged using high resolution X-ray computed tomography. The resulting 3D dataset, with an 11µm voxel size, was analysed to determine the distribution of microstructures preserved in the porphyroblasts. Texturally the porphyroblasts have a large core with a sub-vertical foliation that has a clustered distribution. The mean orientation has a plunge of 18° towards 292.8° and a 95% confidence cone semi-angle of 5.3°. This steep foliation curves into a sub-horizontal foliation. The foliation intersection/inflection axes (FIAs) defined by this curvature have a more tightly clustered distribution. Their orientation has a plunge of 10.6° towards 200.5° and a 95% confidence cone semi-angle of 4.1°. The trend of a second FIA was measured in the median of 17 of the garnets. These axes had a mean orientation of 116.9° with a 95% confidence interval of 114.2° to 119.6°. The clustered distribution of the foliation and FIA data from the core of the porphyroblasts, despite the presence of several later foliation forming events, provide strong evidence that the porphyroblasts have not rotated relative to a fixed geographic reference frame in this sample. The data distribution can be readily explained as variations in the primary fabrics that have been overgrown by irrotational porphyroblasts.

The lack of porphyroblast rotation is explained using the PBIS (progressive, bulk, inhomogeneous shortening) strain model in which deformation partitions into zones of shearing and zones of shortening or no strain. Porphyroblasts are effectively decoupled from the matrix and do not rotate. The FIA orientations are shown to reflect the trend of steep foliations, which is perpendicular to the direction of bulk shortening during horizontal compression, in a succession of steep and flat foliation forming events. An extended deformation history of four foliations is preserved in the porphyroblasts.


# 1 Introduction

In 1968 John Rosenfeld wrote on how curved inclusion trails trapped in garnet porphyroblasts had been underutilized due to a lack of adequate methods of study. He demonstrated how quantitative measurements of axes of curvature could be used in the interpretation of the structural history of the rocks that hosted them. Rosenfeld followed this with a more detailed investigation of these features complete with techniques for measuring them (Rosenfeld 1970). While there has been much debate as to what curved inclusion trails represent and how they formed (Bell 1985, Ikeda et al. 2002, Ilg & Karlstrom 2000, e.g. Schoneveld 1977, Stallard et al. 2002, Williams & Jiang 1999), there was a distinct hiatus in any attempts to apply these features to solving geological problems. Twenty years after Rosenfeld's last communication on the topic, Bell and co-workers introduced the concept of the

Foliation Intersection or Inflection Axis (Bell et al. 1995, FIA`; Hayward 1990). They provided a simplified technique for measuring the axis of curvature (which they call the FIA). This method has been applied to many geological problems including: investigating tectono-metamorphic histories and correlating multiple phases of metamorphism on local and orogenic scales (e.g. Bell et al. 1998, Bell & Mares 1999, Cihan & Parsons 2005, Lee et al. 2000, Sayab 2005, Yeh & Bell 2004); investigating foliation development and folding mechanisms (Bell & Hickey 1997, Timms 2003); arguing for the lack of porphyroblast rotation (Bell et al. 1997, Ham & Bell 2004, Hickey & Bell 1999); studying porphyroblast nucleation and growth relative to deformation (Bell et al. 2003, Bell et al. 2004); reconstructing plate motions (Bell et al. 1995); constraining age dates (Bell & Welch 2002); and investigating pluton emplacement mechanisms and timing (Davis 1993). Using FIAs, these authors have demonstrated that the porphyroblasts have not rotated. If this holds true for most rocks, the value of FIAs to geologists will exceed even Rosenfeld's expectations.

Johnson (1999) raised a series of questions about the measurement of FIAs, mostly regarding measurement errors and the spread of orientations in a single sample. The technique Hayward (1990) described for measuring FIAs yields the average orientation for a sample but cannot measure the orientation of a FIA in an individual porphyroblast. As a result it is difficult to know what the porphyroblast to porphyroblast variation in FIA orientations within a single sample is. The true statistical spread of trends for a sample is unknown. Upton et al. (2003) give a method to determine the spread of values in a single sample using a maximum likelihood approach. However, this technique provides only an indirect measure of the distribution. To allow FIAs to be used to their full potential, questions about the statistical confidence that can be assigned to the determined trends need to be answered. To do this the FIAs in individual prophyroblasts need to be measured in statistically significant quantities so that rigorous analysis can be done.

High resolution X-ray computed tomography (HRXCT) provides a technique that allows inclusion trails to be imaged in intact samples (Huddlestone-Holmes & Ketcham 2005). Previously, serial sectioning of individual porphyroblasts has been used to look at the morphology of the structures preserved inside porphyroblasts (e.g. Johnson 1993b, Johnson & Moore 1996). This is a laborious technique, unsuitable for collating statistically significant amounts of data. It is also difficult to correlate inclusion trail surfaces from section to section, which reduces the accuracy. Using HRXCT, the three-dimensional orientation of FIAs can be measured to a five-degree range in plunge and plunge direction. A large amount of data can be acquired relatively quickly without destroying the sample allowing the application of complimentary techniques if required.

This chapter examines the distribution of FIAs in 58 porphyroblasts from a single sample. The plunge and plunge direction of the FIAs have been measured. Statistical analyses

of the results were applied to describe these data and determine the confidence that can be placed in the measured orientations. By looking at the geometry of the inclusion trails in this sample, inferences can also be made as to what the FIA measurements actually represent, as well as the process that formed them.

## 1.1 What is a FIA?

Foliation inflection or intersection axes (FIAs) are interpreted to be the intersection of successive foliations, or the curvature of one into the next, that have been overgrown by a porphyroblast (Bell et al. 1995, Hayward 1990). Rosenfeld (1970) and others would argue that FIA are the result of the porphyroblast including an active foliation which is causing it to rotate (Fig. 1) and that the FIA is actually the axis of this rotation. Bell et al. (1995) argue that FIAs are the product of overprinting deformation events/foliations and that porphyroblast rotation is not necessary to produce them. The measurement of FIAs makes no inference whether the porphyroblast has rotated or not. If a porphyroblast has not rotated, FIAs within it will still be in their original orientation. If the porphyroblasts has rotated, subsequent foliation forming events will reorient the earlier FIAs. This study will examine whether there was evidence for redistribution in this sample.

FIAs formed by the porphyroblast rotation model will be perpendicular to the direction of movement in the foliation (i.e. the axis of principal strain). FIAs formed by the second of the above models will be perpendicular to the direction of bulk shortening. This is based on the observation that foliations form perpendicular to this direction (e.g. Hobbs et al. 1976, Passchier & Trouw 1996). Bell and Johnson (1989) have argued that foliations in orogenic belts alternate between vertical and horizontal as orogenesis progresses. It follows from this that the orientation of FIAs will be a reflection of the strike of vertical foliations.

## 1.2 The Rotation Debate

The accepted paradigm in the earth sciences until the mid-eighties was that porphyroblasts and other rigid objects rotate with respect to a geographical reference frame during non-coaxial deformation. The rotation is due to the vorticity created by the simple shearing component of the deformation (Lister & Williams 1983, Rosenfeld 1970). Bell and others (Bell 1985, Bell et al. 1989, Bell et al. 1992a, Bell & Johnson 1990, Bell et al. 1992c, Johnson 1993a, Steinhardt 1989) argue that porphyroblasts do not rotate due to the effects of deformation partitioning.

The debate concerns deformation mechanisms. Bell (1981) proposed the PBIS (progressive, bulk, inhomogeneous shortening) strain model, which is based on the concept that the deformation partitions into zones of progressive shearing (shearing) and zones of progressive shortening (shortening or no strain, Fig. 2). A pre-existing porphyroblast will

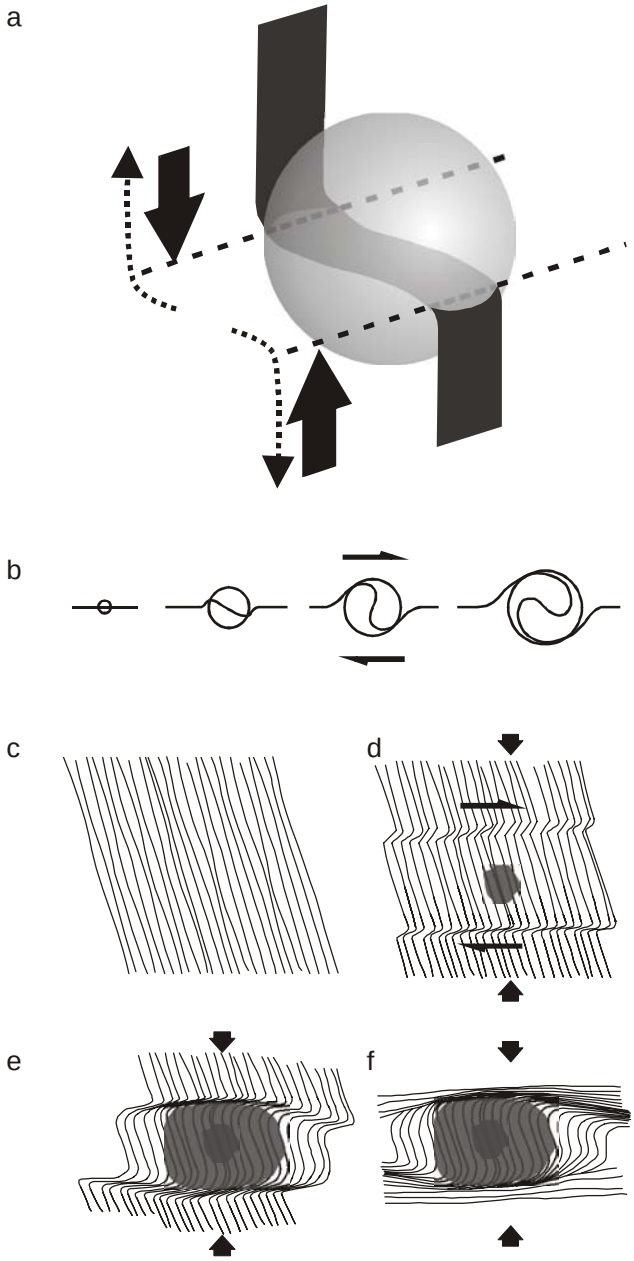


**Figure 1.** The two models for the formation of curved inclusion trails are shown here. In (a), a spherical porphyroblast is shown along with a curved foliation plane that it includes. The dashed lines show the axes of rotation of this foliation plane. The large solid arrows show the shear sense that would have been necessary to form this geometry via porphyroblast rotation, the dotted arrows show the shear sense that would have rotated a flat foliation to the vertical in an irrotational model. A cross section of the rotational model is shown in (b), where a porphyroblast grows while being rotated by shear on the foliation. (c) to (f) show the progressive development of curved trails in the deformation partitioning model. A porphyroblast (grey oval) grows in the crenulation hinge (d), eventually overgrowing the curvature of the sub vertical foliation into the flat foliation (e). The deformation intensifies against the edge of the porphyroblast which has stopped growing (f).

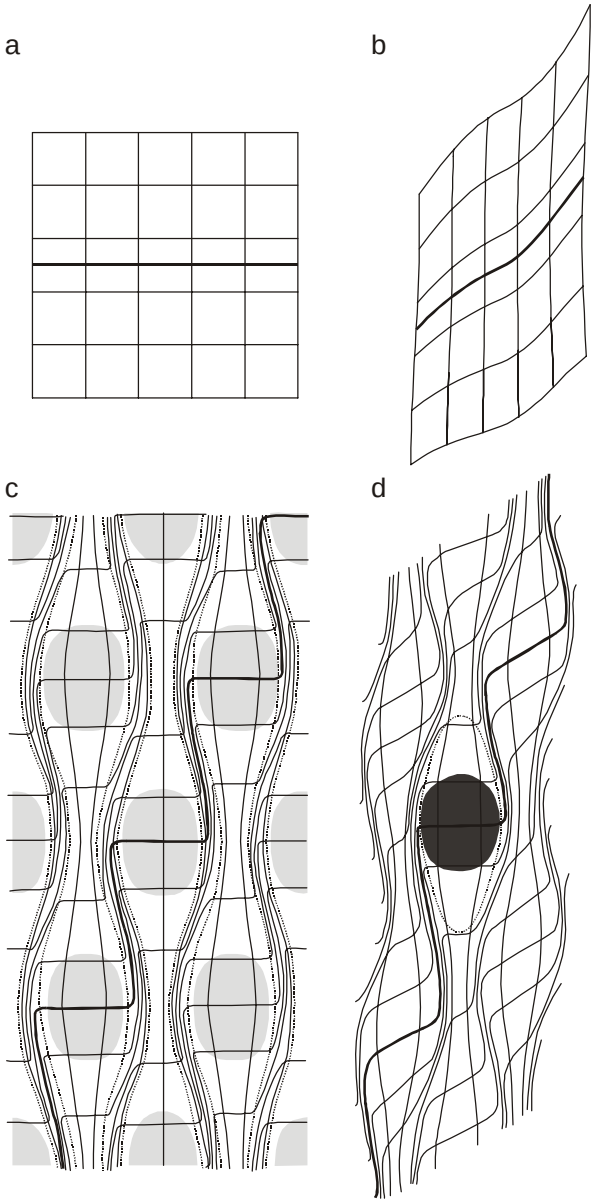


**Figure 2.** This series of strain field diagrams in the $\varepsilon_1\varepsilon_2$ plane demonstrates the development of non-coaxial Progressive Bulk Inhomogenous Shortening (PBIS, Bell 1981). A reference grid is shown in (a) along with a marker band (heavy line). Early in deformation the strain will not have partitioned (b) and coaxial shortening dominates. As deformation progresses (c), the strain partitions into zones of no strain (grey ellipses), zones of shortening (between the ellipses and the dotted lines) and zones of shearing (between the dotted lines). In (b) and (c) the dark grey ellipse represents a porphyroblast which causes strain to partitions around it throughout deformation.

partition the deformation so that it is in a zone of no strain (Fig. 2d). It is effectively decoupled from the matrix and does not rotate. This concept has formed the central plank of the non-rotation argument since first used in this way by Bell (1985). The majority of theoretical models for rigid body rotation are based in hydrodynamics theory (e.g. Samanta et al. 2002a) and, unsurprisingly, these models predict that a rigid body in a fluid undergoing a deformation with a simple shearing component will rotate. Significantly, the rotational models do not account for

the great wealth of data that suggests that porphyroblasts do not rotate (e.g. Aerden 2004, Aerden 1995, Bell & Chen 2002, Bell & Hickey 1999, Evins 2005, Hayward 1992, Johnson 1990, Jung et al. 1999, Steinhardt 1989).

Recently, several papers describing the results of analogue modeling cast doubt on the validity of hydrodynamic models (Aerden 2005, Ceriani et al. 2003, Mancktelow et al. 2002, Stewart 1997, ten Grotenhuis et al. 2002). Two problems have been identified, firstly the applicability of a viscous fluid as an analogue to rocks that are anisotropic and heterogeneous. Secondly, the nature of coupling between the matrix and porphyroblast appears to have a significant effect. It is clear from the literature that the scientific community still has no firm consensus as to whether or not curved inclusion trails form by rotation. How these data fit with both of these hypotheses will be investigated.

## 1.3 Geological Setting

The oriented sample selected for this study comes from southeast Vermont, where the pioneering work on curved inclusion trails by Rosenfeld (Rosenfeld 1968, Rosenfeld 1970) was done. Sample V209 was collected from the Cram Hill Formation in southeastern Vermont and is ideally suited to this kind of study because it has a high density of garnet porphyroblasts, most with well-developed inclusion trails (Fig. 3). It is a carbonaceous pelite that has been metamorphosed to amphibolite facies and contains quartz, muscovite, garnet, biotite, calcite, ilmenite and trace epidote. Fine graphite is present throughout the rock as a dusting of grains that, in places, form density bands. At hand sample scale quartz and mica rich bands are observed. Inclusion trails within garnet are composed of quartz, ilmenite, graphite, magnesian siderite, hydrated iron oxide and pyrophyllite.

## 1.4 Previous Work

Bell et al. (1998) document three separate FIAs for sample V209. Oldest to youngest (core, median and rim/matrix), these trend at 45˚, 110˚ and 30˚ respectively (relative to magnetic north, which is 14˚ west of true north at the sample locality) and are assigned to regional FIA sets 1, 2 and 4 respectively. In the same study Bell et al. (1998) reported FIAs for 88 samples from the region where sample V209 was collected. They distinguished four distinct FIA sets in the region, trending SW-NE, W-E, NNW-SSE and SSW-NNE (sets 1 to 4 respectively, 1 youngest, 4 oldest). Some examples of how these data have been used include distinguishing multiple phases of metamorphism (Bell et al. 1998), constraining age dates (Bell & Welch 2002) and investigating regional patterns of deformation partitioning (Bell et al. 2004).

**Figure 3.** Photomicrograph of sample V209 showing its garnet density and inclusion trails. Note that the bulk of the trails are steep in the core of the garnets, with a clockwise asymmetry. The section is oriented east-west looking north. The short edge of the image is approximately 11mm.

# 2 Methods

## *2.1 The Asymmetry Method*

Hayward (1990) introduced the asymmetry method for determining FIA orientations which was later refined by Bell et al. (1995). Using the horizontal plane as a reference, the strike of the FIA is determined first. Six vertical thin-sections striking at 30˚ increments are prepared for each sample. The asymmetry of curved inclusion trails are noted for porphyroblasts in each thin-section viewed in the same direction (clockwise about a vertical axis). The trend of the FIA is constrained to a 30˚ interval over which the observed asymmetry flips. Two additional vertical thin-sections are cut to further constrain the trend to a 10˚ interval (Figs. 4 and 6). A similar procedure is followed to obtain the plunge of a FIA; a series of thin-sections dipping in the vertical plane that contains the trend of the FIA are prepared, and again, the interval over which the asymmetries flip is determined.

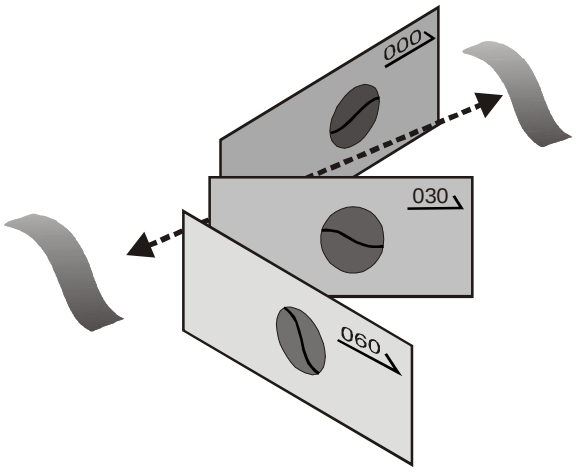


**Figure 4.** This figure illustrates the asymmetry method. In this case the FIA is oriented at approximately 015°. Vertical thinsections striking at 000°, 030° and 060° are shown – note the flip in asymmetry of the inclusion trails in the grey "porphyroblasts" from clockwise to anti-clockwise between 000° and 030°. Extra sections between these two would allow the FIA to be constrained further. A similar process can be used to define the plunge of the FIA.

### 2.1.1 Asymmetry Method Statistical Analysis

Some work has been published that discusses the statistical analysis of FIA data collected in a region (Bell et al. 1998, Yeh & Bell 2004). However, apart from reporting the range over which the flip in asymmetry occurs, there has been no way of describing the confidence of an individual FIA measurement until recently. Upton et al. (2003) developed a maximum likelihood estimation (MLE) approach to fit a cyclic logistic regression to asymmetry data allows the FIA orientation and a shape parameter to be determined. The shape parameter, β, describes how rapidly the asymmetry of inclusion trail curvature changes as the FIA orientation is approached. This allows a confidence interval to be calculated. This technique has been greatly improved in Chapter 3 using bootstrapped estimates of the model parameters. These methods have been applied in analysing the asymmetry data described.

## *2.2 High Resolution X-ray Computed Tomography*

High resolution X-ray computed tomography (HRXCT) is a technique that can be used to image the structures preserved within solid objects such as rocks. It is an adaptation of medical X-ray computed tomography (X-ray CT) with the benefits of increased resolution (<10μm cf. 2-3m), longer scan times and higher X-ray energies (up to 400 keV). Recently this technique has been applied to imaging inclusion trails in garnet posphyroblasts (Bauer et al. 1998, Ikeda et al. 2002). In chapter 1 of this thesis the technique is described in full, demonstrating the detail that can be seen in images produced by HRXCT and comparing them with more familiar polarizing microscope images and compositional maps collected on an electron microprobe.

In summary, HRXCT in geological materials measures the attenuation of X-rays as they pass through different minerals in the sample. Minerals with a higher average atomic number (Z) and higher density will attenuate more X-rays, and are traditionally assigned lighter shades in a greyscale image (like bones in an X-ray). The amount of attenuation is in part related to the energy of the X-rays. Because the X-ray sources are polychromatic, images constructed using HRXCT are qualitative. Phases such as quartz, the feldspars, calcite and micas have significantly lower attenuation coefficients (a measure of the level of X-ray attenuation) than garnet, while iron oxides and REE phases such as monazite are significantly more attenuating. As a result, HRXCT images provide clear differentiation between matrix, garnet and inclusions within the garnet. The three-dimensional datasets created by HRXCT are actually a stack of two-dimensional slices taken through the object of interest. The slices are typically scanned with a fan of X-rays passing through the object as it is turned through 360º and data is collected at rotational increments (views). An image for each slice is reconstructed from these data and they are stacked together to form the three-dimensional dataset.

### 2.2.1 HRXCT Scan Parameters

To prepare the sample for HRXCT, two horizontally oriented slabs 30mm thick were cut from the top and bottom of the specimen. Two vertical drill cores 11mm in diameter were taken from each slab (Fig. 5). To ensure that the orientation of the drill cores was preserved, a north-south groove was made in the top surface of the slabs before coring, and a piece of wire with a notch at the northern end was glued into the groove after coring. This provided an orientation marker that could be clearly imaged by X-ray CT. Cylindrical drill cores are ideal for X-ray CT analysis.

| **Parameter** | **Value** | **Parameter** | **Value** |
|---|---|---|---|
| Source Voltage (keV) | 150 | Voxel size (μm x μm x μm) | 10.7 x 10.7 x 13.1 |
| Beam Current (mA) | 0.2 | | |
| Spot size (μm) | 30 | Image scale | 16-bit |
| Slice thickness (mm) | 0.0131 | Views per 360˚ | 1600 |
| Spacing of slices (mm) | 0.0131 | Time per view (ms) | 133 |
| Number of slices | 918 | Time per slice* (min) | 1.3 |
| Scanned height (mm) | 12.0 | Wedge | SMT** |
| Field of view (mm) | 11.0 | Offset | none |
| Slice resolution (pixels x pixels) | 1024 x 1024 | Source to Object Distance (mm) | 38 |

* Data for 27 slices acquired simultaneously

** SMT – sodium metatungstate solution mixed to a density of 1.19g/cm$^3$

**Table 1.** X-ray CT scan parameters used for each of the four cores analysed. See text for further discussion.

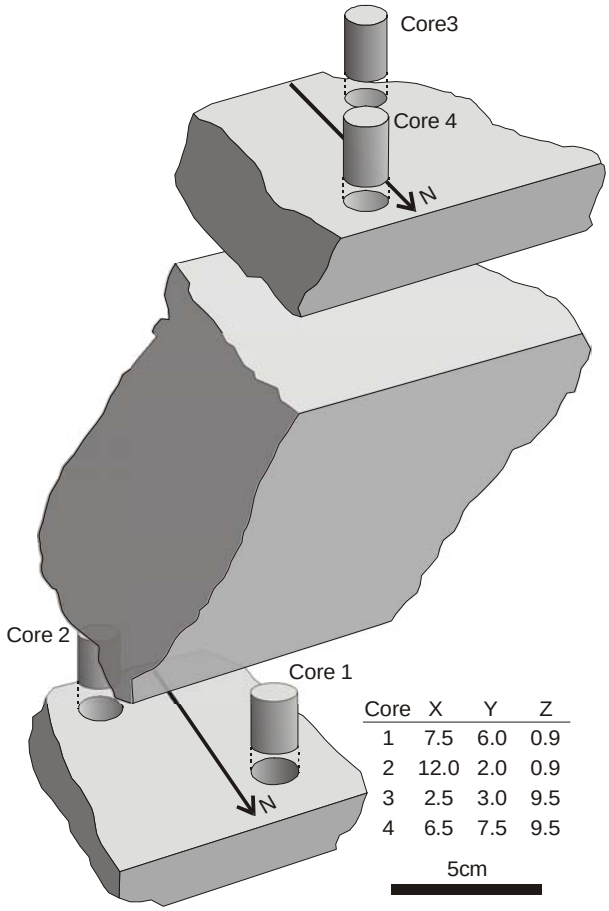


**Figure 5.** Schematic showing relative positions of the four drill cores analysed in this study. The table shows the coordinates of the centre of the drill cores in a coordinate system originating at the lower southwest corner of a box bounding the sample.

The scanner used for this study is housed in the University of Texas HRXCT Facility. Table 1 shows the scan parameters used in this study. Each drill core was scanned along a twelve millimetre axial length, with the data for all four drill cores collected in approximately ten hours. Image reconstruction was done as a separate process after acquisition by applying back-projection using a Laks filter. Each image is 1024 by 1024 pixels of 16-bit data, and there are 918 images or slices for each drill core making for a total dataset of over 7 GB.

### 2.2.2 FIAs and Foliations from HRXCT

The data were analysed using the OpenDX (www.opendx.org) software package. Firstly, a low resolution dataset was created by taking every fourth slice and downsampling it to 8-bits and 256 x 256 pixels. The locations of the centres of the garnet porphyroblasts were measured using this dataset. Subsets were then made of the full resolution dataset centred on each garnet with dimensions slightly greater than the garnets maximum. These subsets were used to reduce the computing time involved in analysing these data. The resulting volumes were

sliced vertically through individual porphyroblasts in the same manner that vertical thin-sections are taken for a rock using the asymmetry method. These slices could be made through any part of the garnet to ensure that they passed through inclusion rich zones from which the asymmetry of curvature could be determined. Once the trend of the FIA was identified, slices dipping in a plane parallel to this trend were made to determine its plunge.

To determine the trend of foliations preserved in the cores of the garnet, the strike of inclusion trails was first measured in a horizontal slice through the core of the garnet. The pitch of the trails was then measured in three vertical slices, one perpendicular to the strike and two at 40º to the strike. The plane of best fit for these data was then calculated. The reasons for following the approach of using 2-D slices of a 3-D dataset in preference to working directly with the 3-D data are explained in the discussion.

### 2.2.3 HRXCT Data Statistical Analysis

The statistical analysis of the three-dimensional distribution of data measured in this sample followed the techniques described in Fisher et al. (1987) for analysing circular data. FIA data and poles to foliations are considered to be undirected lines, or axial data, and must be treated as such. Initial investigations were made using graphical methods (stereoplots, colatitude and longitude plots) together with calculation of the eigenvalues and eigenvectors of the orientation matrix. The eigenvalue method provides the mean orientation as well as describing the shape of the distribution (Woodcock 1977, Woodcock & Naylor 1983). This is important in determining whether the data are clustered or have a girdle distribution. The next stage involved parametric analysis – if the data are clustered, a Watson bipolar model (the spherical equivalent of a normal distribution) can be fitted; if it has a girdle distribution, a Watson girdle model would be used. The advantages of applying a parametric model to the data are that tests for discordance can be done and, if appropriate, a conical confidence interval determined.

As well as a detailed analysis of the total dataset, exploratory analysis was done on data from each of the four drill cores to see if there was a significant difference between them. The data were tested, both graphically and formally, to see if each of the four drill cores samples the same population.

For trend data, the techniques described in Fisher (1993) for analysis of circular data were applied. A similar approach to that used for the spherical data was used with a graphical analysis using rose diagrams and calculation of a mean and confidence interval. Parametric tests were not performed.

Tests for correlation between the orientation of the FIAs, the orientations of foliations in the core of the garnets and the diameter of the porphyroblasts were also performed. For the spherical data, the techniques for testing for correlations between two random unit axes and between a random unit axis and another variable that are described in Fisher et al. (1987) were

employed. For the trend data (i.e. circular), the tests for a T-linear association outlined in Fisher and Lee (1983) and Fisher (1993) were used. These tests calculate a correlation coefficient "pt" that give an indication of the strength of any correlation. For the test to check for any dependency of FIA trends on garnet diameter, the diameter was first converted into a radial measurement by the equation $2 \times atan(diameter)$ which allows the standard T-linear test to be used.

Modification of the analysis of these data due to their grouped nature was not performed because the 5º interval is small enough that it is not necessary (Upton & Fingleton 1989). In reporting eigenvalues and eigenvectors, t1 is taken to be the smallest eigenvalue and t3 the largest, or principal axis, as in Fisher et al. (1987).

# 3 Results

## *3.1 General Description of Trails*

Sample V209 has almandine-rich garnet porphyroblasts with two distinct textural zones: firstly, a broad core with a moderate density of elongate quartz, ilmenite grains, fine graphite, magnesian siderite and bands of hydrated iron oxide with pyrophyllite and quartz inclusions; and secondly, a fine rim with very few inclusions except graphite. The hydrated iron oxide/clay bands are interpreted to be the result of alteration along inclusion rich bands that probably represent some form of compositional layering in the rock prior to garnet growth. The composition of the precursor inclusions cannot be determined. The orientation of these bands does not appear to have been changed by the alteration process. Inclusion trail density is higher in porphyroblasts that lie in the sample's quartz rich bands. The garnet porphyroblasts show well-developed crystal faces in the mica rich bands only.

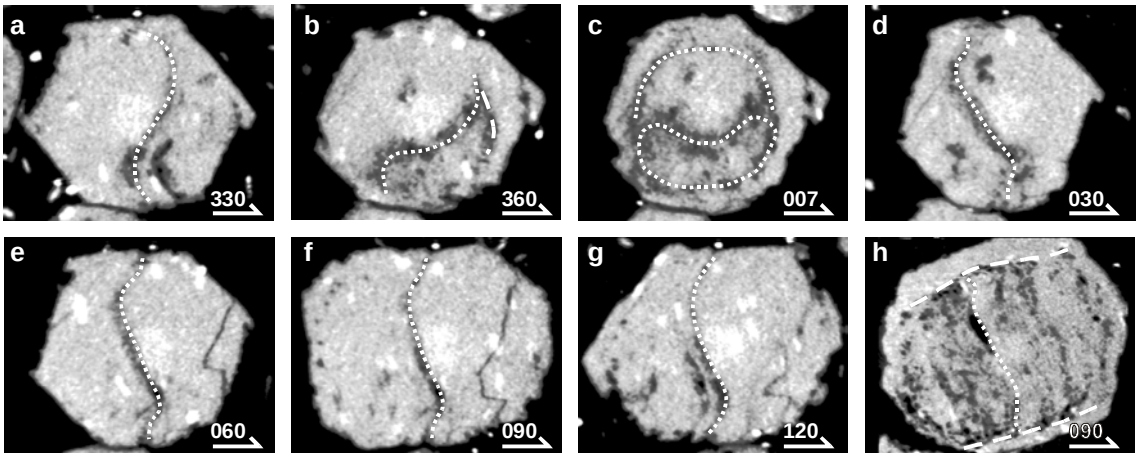


**Figure 6.** A series of vertical sections through the X-ray CT data for garnet 27 in drill core 1 (a-g) showing the asymmetry flip in the core at 007° from anticlockwise to clockwise. Note the closed loop pattern in (c), which is on the FIA. The flip in rim asymmetry is subtler and can be recognized by the change from "stair case" to "accumulating" trails between the 090° and 120° sections. The horizontal truncation in garnet 7 in drill core 3 is shown in (h).

Characteristically the inclusion trails in the core of the garnet porphyroblasts (which generally extends to 70 – 80% of the porphyroblasts' radius) are sub-vertical with an east-southeast dip direction. These trails curve smoothly in a top to the east sense by a maximum of 110º. They have a subtle doubly curving non-cylindrical geometry that results in closed loop structures in sections parallel to them (Fig. 6). Depending on the orientation of the section, a reversal in the asymmetry at the edge of the core trails is observed in some garnets. This flip occurs over a very short distance relative to the extent of the core and the trails are truncated at the transition to the rim in some garnets, whether there is a rim growth or not (Fig. 6). The graphitic inclusion trails in the rim are sub-horizontal and curve into the vertical matrix foliation. Distinct FIA orientations can be determined for the core, median and rim/matrix. However, as the rim trails are fine and graphitic, they could not be analysed using HRXCT and will not be considered further. All data are reported relative to magnetic north unless otherwise noted. The magnetic deviation at the sample locality was 14° west at the time that the sample was collected.

## *3.2 The Asymmetry Method*

Eighteen sections were cut at 10° intervals from 000° to 170°. The asymmetry of curvature was recorded for every garnet where it was unambiguous (the data are presented in appendix 1). Ambiguities were due to millipeding, poor inclusion density, fracturing, alteration, off centre cuts or a combination of these factors. The core and median FIAs were determined to be at 25° and 115° respectively. For the core FIA, both asymmetries are observed in the 350° (170°), and 000° to 060° sections (see Fig. 7). Both asymmetries were observed in the 090° to 140° sections for the median FIA. Using the maximum likelihood estimation approach described in Chapter 3, the core FIA trend was determined to be 24.7º with a 95% confidence interval of 21.5° to 27.9° and the median FIA trend was determined to be 116.3°, with a 95% confidence interval of 112.8° to 119.8°.

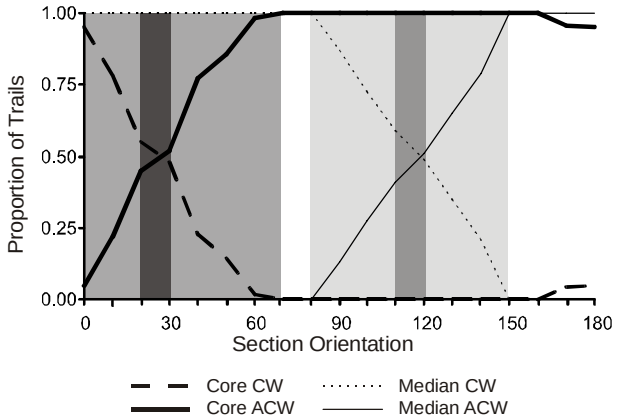


**Figure 7.** Probability plot for asymmetry data collected from thin-sections. Lighter grey areas show region over which both asymmetries are observed, dark grey bars indicate the interval over which the dominance of one asymmetry gives way to the other. See appendix 1 for the raw data.

## *3.3 HRXCT Data*

### 3.3.1 FIA Data

FIA orientations for the core part of the garnet, which were determined to a 5° interval for both plunge and plunge direction from a total of 58 garnets, are shown in Fig. 8 a and b and listed in appendix 2. The stereonets shows that these data have a clustered distribution that may be slightly skewed. The mean FIA orientation for these data plunges at 10.6° towards 200.5° (see table 2). Eigenvalue methods (Woodcock 1977, Woodcock & Naylor 1983) confirm that the data are clustered with moderate strength (table 2 and Fig. 9). The data can be shown to be symmetrical using the tests described by Fisher et al. (1987) and have a 95% confidence cone with a semi-angle of 4.1°. Colatitude and longitude q-q plots performed as goodness of fit tests for the Watson distribution, (Fig. 10) indicate that the data are well represented by a Watson distribution. The colatitude q-q plot (Fig. 10b) appears to curve up slightly at higher values, but it does not deviate markedly from a straight line. This is confirmed by a formal test based on the modified Kolmogorov-Smirnov statistic, $M_B(D_N)$, with a value of 0.614 which is well below the critical value at 95% confidence of 1.09 (Table 2b.).

| | | eigenvalues (normalized) | | | eigenvectors | | | | | |
|---|---|---|---|---|---|---|---|---|---|---|
| **Core FIAs** | **n** | **t1** | **t2** | **t3** | **t1** | **t2** | **t3*** | **K (shape)** | **C (strength)** | **95% Conf. Cone** |
| **All Data** | 58 | 0.033 | 0.058 | 0.909 | 0.2 → 110.4 | 79.4 → 19.3 | 10.6 → 200.5 | 4.92 | 3.31 | 4.15 |
| **Drill Core 1** | 24 | 0.022 | 0.062 | 0.916 | 5.7 → 110.1 | 76.0 → 356.6 | 12.8 → 201.4 | 2.60 | 3.74 | 6.14 |
| **Drill Core 2** | 10 | 0.008 | 0.046 | 0.946 | 8.1 → 294.3 | 72.0 → 50.2 | 16.0 → 202.0 | 1.71 | 4.79 | i.d. |
| **Drill Core 3** | 8 | 0.013 | 0.068 | 0.920 | 44.9 → 312.8 | 41.8 → 106.1 | 13.7 →208.7 | 1.55 | 4.29 | i.d. |
| **Drill Core 4** | 15 | 0.028 | 0.054 | 0.918 | 38.2 →284.1 | 51.8 → 101.5 | 1.3 → 193.1 | 4.41 | 3.48 | i.d. |
| **Foliations** | | | | | | | | | | |
| **All Data** | 55 | 0.045 | 0.082 | 0.873 | 22.8 → 194.9 | 60.3 → 57.5 | 18.0 → 292.8 | 3.94 | 2.97 | 5.31 |
| **Drill Core 1** | 22 | 0.024 | 0.051 | 0.925 | 4.2 → 21.4 | 81.5 → 141.2 | 7.3 → 290.9 | 3.77 | 3.66 | i.d. |
| **Drill Core 2** | 10 | 0.018 | 0.034 | 0.949 | 40.8 → 179.1 | 32.3 → 56.0 | 32.4 → 302.3 | 5.29 | 3.97 | i.d. |
| **Drill Core 3** | 8 | 0.010 | 0.054 | 0.936 | 7.4 → 216.1 | 59.8 → 113.2 | 29.1 → 310.2 | 1.68 | 4.56 | i.d. |
| **Drill Core 4** | 15 | 0.043 | 0.061 | 0.896 | 39.2 → 25.8 | 45.6 → 172.4 | 17.4 → 281.0 | 7.66 | 3.03 | i.d. |

**Parametric Analysis (3-D)**

| | **n** | **mean** | **95% Cone** | **k** | **k upper** | **k lower** | **Pn** | **Mb(Dn)** |
|---|---|---|---|---|---|---|---|---|
| **Core FIAs** | 58 | 10.6 → 200.5 | 4.15 | 11.621 | 13.774 | 8.1773 | 4.05 | 0.61358 |
| **Foliations** | 55 | 18.0 → 292.8 | 5.31 | 8.6024 | 9.947 | 5.8206 | 5.32 | 1.1821 |
| **Critical Values (95% confidence)** | | | | | | | < 5.99 | < 1.09 |

* mean orientation of FIAs and poles to foliation data.

**Table 2.** Statistical analysis of spherical data. "K" and "C" are shape parameters after Woodcock (1977). Parametric analysis is done for a Watson bipolar model. Pn is a symmetry and longitude goodness-of-fit test; Mb(Dn) is a colatitude goodness-of-fit test for this distribution. i.d. stands for insufficient data for the test to be meaningful. See text for further discussion.

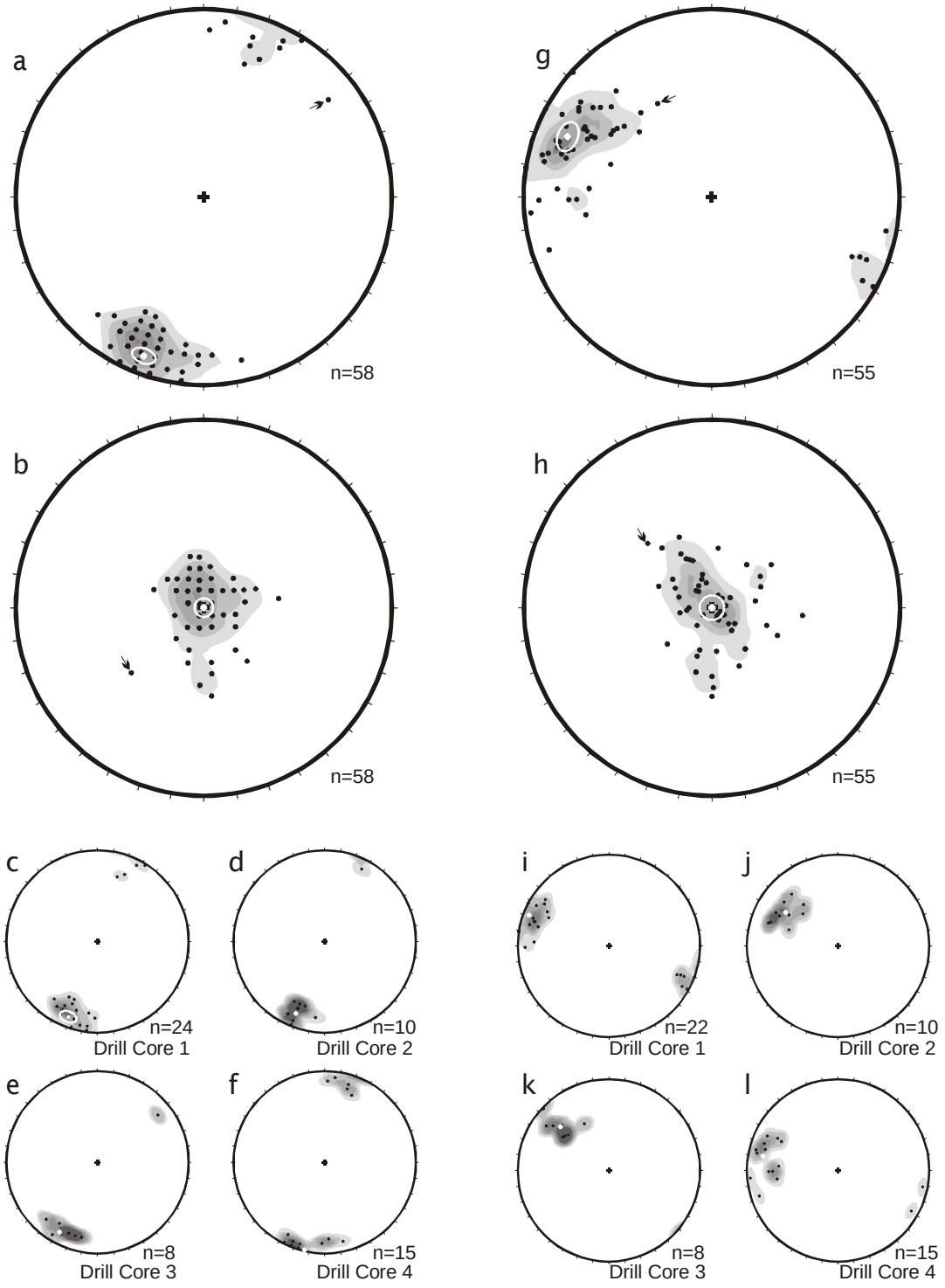


**Figure 8.** Equal-area stereonets of FIAs (a-f) and poles to foliation (g-j) in the cores of the prophyroblasts. (a-b) and (g-h) are the whole datasets with the data rotated so that the mean orientation is 90° → 000° in (b) and (h). This allows the shapes of the distributions to be seen more clearly. The FIA data shows a moderately clustered distribution while the foliations are more dispersed with a slight girdle character. The smaller stereonets show the data recorded for the individual drill cores, as labelled. See text for further discussion. Contouring done using Dips version 5.0 (www.rocscience.com) with 5% contour intervals using the Schmidt distribution method. The white crosses show the mean orientations in each projection and white circles the 95% confidence cone where calculated. Small arrows point to garnet 3 in drill core 3. See text for discussion.

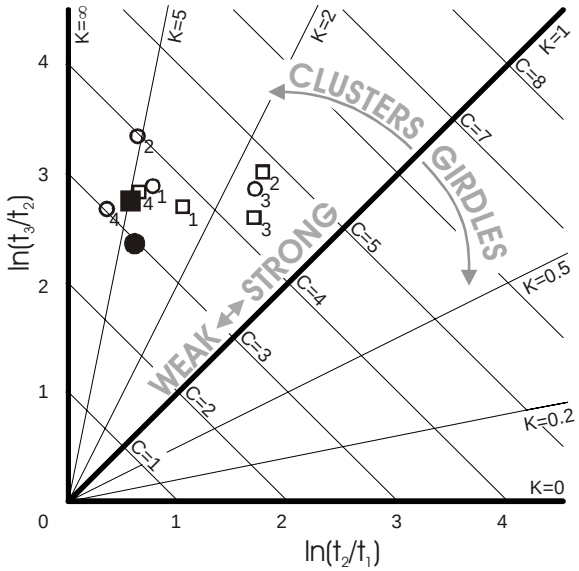


**Figure 9.** Eigenvalue ratio graph of Woodcock (1977) for core FIA (squares) and foliation (circles) data for the whole dataset (solid) and individual drill cores (open, numbered). This plot shows Woocock's shape (K) and strength parameters (C). Note that all datasets have similar values, with the exception of drill cores two and three.

The colatitude q-q (Fig. 10 b) plot also shows that the data from the four drill cores form part of the same distribution (in that the data all lie on the same trend), even though their mean orientations differ slightly. This was confirmed by a formal test with an $N_r$ statistic value of 3.30, which is well below the critical value at 95% confidence of 12.58. Stereonets for each drill core are shown in Fig. 8c-f and results of eigenvalue analysis are given in table 2 and Fig. 9. Data from the four drill cores have similar shape and strength parameters to the whole dataset. Drill cores two and three, while still clustered, approach girdle distributions. Drill core three varies more in dip than dip direction and drill core four varies more in dip direction than dip. However, both have relatively low sample counts. Drill core four has a much gentler plunge than the others do.

The trend data for the core FIA was also analysed for direct comparison with the traditional methods of FIA measurement and the results are presented in table 3. There is good agreement between the asymmetry method, the MLE approach and the mean value from the HRXCT data.

The trend of the median FIA could be measured in only seventeen porphyroblasts (appendix 2, Fig. 11) as it occurs over such a short interval of the garnet radius; the resolution of the HRXCT data is not high enough to resolve such fine features. It was not possible to determine plunges, as the region in which the flip in asymmetry occurred was difficult to intersect with horizontal to sub-horizontal sections. The mean trend of the data is 116.9° with a 95% confidence interval of 114.2° to 119.6° (table 3). The absolute range of data is only 20°. This agrees well with the results of the asymmetry method and MLE approach (table 3). The

median for the four drill cores was not analysed individually because there was insufficient data to do so.

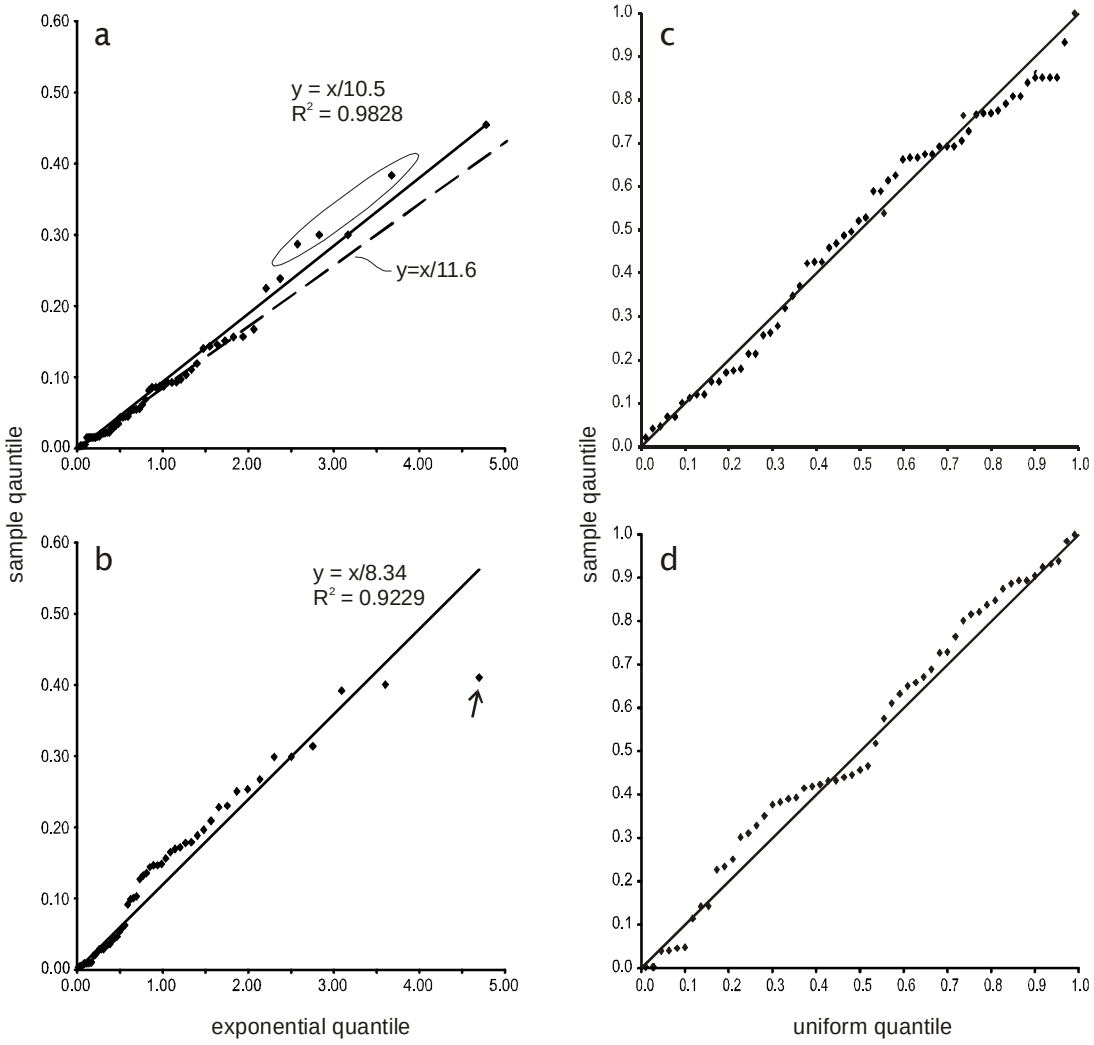


**Figure 10.** Colatitude (a and b) and longitude (c and d) probability plots for core FIA (a and c) and foliation (b and d) data to check the goodness of fit of the Watson bipolar distribution to these data. These plots indicate that the assumption that the Watson bipolar distribution fits these data is reasonable. The three points circled in the FIA colatitude plot, and the point marked with an arrow in the foliation colatitude plot may be discordant as they lie some distance from the line of best fit. See test for discussion of formal tests. The dashed line in (a) shows the trend using y=x/k where k is the maximum likelihood estimate for this dataset. The longitude plot also gives an indication as to whether the data from the four drill cores are all from the same distribution. These plots show no departure from a 1:1 line indicating that these data are all from the same distribution.

| Core FIAs | n | R | R/n | mean | 95% upper | 95% lower | interval |
|---|---|---|---|---|---|---|---|
| **All Data** | 58 | 53.86 | 0.93 | 20.60 | 23.40 | 17.81 | 5.59 |
| **Core 1** | 24 | 22.84 | 0.95 | 21.52 | 25.17 | 17.86 | 7.31 |
| **Core 2** | 10 | 9.81 | 0.98 | 22.05 | 25.12 | 17.89 | 7.22 |
| **Core 3** | 8 | 7.27 | 0.91 | 29.17 | 40.26 | 19.84 | 20.41 |
| **Core 4** | 15 | 13.81 | 0.92 | 13.03 | 19.48 | 5.87 | 13.60 |
| **Asymmetry Method** | | | | 25 | 0* | 70* | |
| **Max. Likelihood Technique** | | | | 24.68 | 27.88 | 21.47 | 6.41 |
| | | | | | | | |
| **Median** | | | | | | | |
| **FIA** | 17 | 16.70 | 0.98 | 116.91 | 119.64 | 114.17 | 5.47 |
| **Asymmetry Method** | | | | 115 | 80* | 150* | |
| **Max. Likelihood Technique** | | | | 116.3 | 119.83 | 112.75 | 7.08 |
| | | | | | | | |
| **Foliations** | | | | | | | |
| **All Data** | 55 | 47.50 | 0.87 | 23.37 | 27.34 | 19.40 | 7.94 |
| **Core 1** | 22 | 20.88 | 0.95 | 21.01 | 25.13 | 16.68 | 8.45 |
| **Core 2** | 10 | 9.22 | 0.92 | 32.60 | 41.06 | 24.64 | 16.42 |
| **Core 3** | 8 | 7.71 | 0.96 | 40.52 | 47.12 | 36.08 | 11.04 |
| **Core 4** | 15 | 13.24 | 0.88 | 10.99 | 20.27 | 2.45 | 17.82 |

*Asymmetry method confidence interval is the range over which both asymmetries are observed rather than 95% confidence interval.

**Table 3.** Statistical analysis of circular data (i.e trends/strikes). Where n <25, 95% confidence interval is calculated using bootstrapping techniques with 20,000 resamples.

### 3.3.2 Foliation Data

The orientations of the foliation in the centre of the garnet porphyroblasts are shown in Fig. 8c and d and listed in appendix 2. They could be measured in all but three of the porphyroblasts for which FIAs were measured; the trails in those three were too smoothly curving or disjointed to measure. These data show a similar distribution pattern to the FIA data although they are less strongly clustered. The mean orientation of the pole to the foliation plunges at 18° towards 292.8° with a 95% confidence cone semi-angle of 5.3°. Eigenvalue methods confirm the observation of a more weakly clustered distribution (table 2 and Fig. 9) than for the FIA data. The data can be shown to be symmetrical using the tests described by Fisher et al. (1987) and has a 95% confidence cone with a semi-angle of 5.3°. While colatitude and longitude q-q plots (Fig. 10) suggest that the Watson bipolar model may be an acceptable description of the data, the formal colatitude test does not hold at the 5% confidence level with an $M_B(D_N)$ value of 1.18 (table 2b). The last point on the colatitude plot (core 3, garnet 3; marked with arrow in Figs. 8b,g,h and 10b) lies some way off the best fit line suggesting it may be discordant. As the data cannot be confidently approximated by a parametric distribution it is not possible to do a formal discordance test. However looking at the stereonets (Fig. 8c and d) this point does not lie at a significant distance from the rest of the population and may be assumed to be part of it.

As for the FIA data, a colatitude q-q plot (Fig. 10 d) shows that the data from the four drill cores all form part of the same distribution. In this case the $N_r$ statistic value is 8.543, which is below the critical value mentioned in 3.3.1. Stereonets for each drill core are shown in Fig 8i-l and results of eigenvalue analysis in table 2 and Fig. 9. The four drill cores have similar shape and strength parameters to the whole dataset. Drill core three shows data approaching a girdle distribution varying more in dip than dip direction.

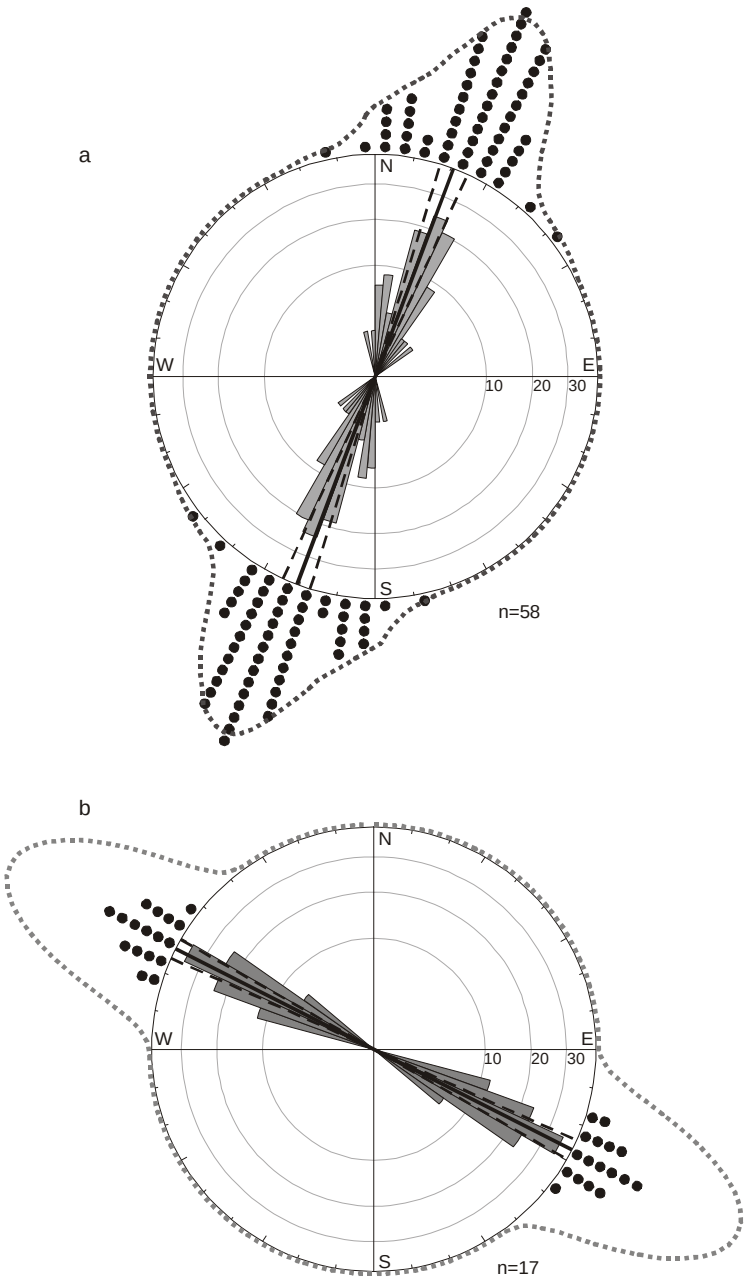


**Figure 11.** Raw data plot, rose diagram and non-parametric density estimates of core (a) and median (b) data. The rose diagram has 5° bins with a scale proportional to the square root of the relative frequency; the dotted lines are non-parametric density estimates (Fisher, 1993) with a smoothing parameter of 0.467 for the core data and 0.627 for the median data. The mean FIA orientations are shown with the solid black line and the 95% confidence interval with the dashed lines.

| Correlation Analysis<br>Spherical Data | Test Value | Critical Value | Significance Prob. | Correl. Coef. |
|---|---|---|---|---|
| **FIA vs Size** | 2.12 | 7.82 | 0.549 | na |
| **FIA vs Foliation Orientation** | 16.18 | 16.92 | 0.063 | na |
| **Circular Data** | **Test Value** | **Critical Value** | **Significance Prob.** | **Correl. Coef.** |
| **FIA trend vs size** | 0.34 | 1.96 | 0.37 | na |
| **FIA vs Fol'n trends** | 2.97 | 1.96 | 0.0015 | 0.68 |

**Table 4.** Results of correlation analyses. Only FIA trend versus foliation trend show a statistically significant correlation. See text for a discussion of correlation tests used.

### 3.3.3 Correlations

There is no correlation between garnet size and FIA orientation or between the FIA orientations and the poles to the foliations, with the hypothesis that there is no correlation holding at the 95% confidence level in both cases (see table 4). However there is a good correlation between the *trends* of the FIA and the foliations, with the probability significance that there is no correlation being less than 1%.

# 4 Discussion

## *4.1 FIAs from HRXCT*

Chapter 1 demonstrated that HRXCT is capable of imaging inclusion trails in garnet porphyroblasts and here the technique has been applied to analysing the FIA orientations within different portions of a sample. The method used to measure the orientations did not use a 3-D version of the data (Fig. 7, Chapter 1), but rather used multiple 2-D slices. This approach was taken because measuring the orientation of a FIA is difficult in a 3-D dataset. Unless there was a continuous inclusion trail running through the centre of each of the porphyroblasts it would be difficult to determine where the axis went, particularly if the axes are not truly linear, due to parallax error or difficulty in aligning individual inclusions. An immersive 3-D visualization environment would help to address this issue but at this these are not readily available. By taking numerous 2-D slices these issues are alleviated. The HRXCT data can be sliced at any orientation and through any part of the porphyroblast. This allows the asymmetry method to be used. Multiple sections can be taken at each orientation, spaced fractions of a millimetre apart, so that the asymmetry can be determined in that orientation with a high degree of confidence. Cut effects can be avoided by taking sections at or near the centre of the porphyroblasts. In some instances the FIA appear to have a curvilinear nature (see below for a discussion of the significance of this). The 2-D technique used here allows the orientation for the centre part of the FIA to be measured, and helps to average out any variation within a porphyroblast.

The range over which the asymmetry flip could be determined varied from porphyroblast to porphyroblast, but was less than 5° in all cases. This lack of certainty is the result of poor inclusion trail density, the curvilinear nature of the axes and limitations in the resolution of the HRXCT technique. For these reason, all asymmetries were recorded at 5° intervals. A potential problem with this is the case where the FIA lies exactly on a multiple of 5°. In this case the inclusion trails would form a coaxial pattern and no asymmetry would be apparent. To deal with this situation a FIA that lies at a multiple of 5° would be included in the lower 5° interval. For example, if a clockwise asymmetry was observed in the 25° section and the 30° orientations displayed a coaxial pattern, the FIA would be assigned to the 25° to 30° interval. However, this did not occur with this dataset.

## *4.2 Formation of Curved Inclusion Trails*

As discussed earlier, there are two competing hypotheses for how curved inclusion trails form; the first states that the porphyroblasts have rotated relative to a fixed geographic reference frame during shearing (referred to as the rotation hypothesis from here on); the second states that the porphyroblasts have not-rotated relative to a fixed geographic reference frame and that the curvature is a result of the porphyroblasts overgrowing crenulated foliations early during the formation of one, or a succession of, crenulation cleavages (the non-rotation hypothesis). The following discussion will examine the data presented in this paper to see if either one of these models is favoured. A fixed geographic reference frame is assumed in the following discussion.

### 4.2.1 Geometry of Inclusion Trails

Detailed examination of the 3-D geometry of the inclusion trails in this sample was not an aim of this study. However, the inclusion trails in the cores of most of the porphyroblasts have a doubly curving non-cylindrical geometry. This indicates the garnet porphyroblasts were rotating relative to the foliation that was included as they grew. If the non-rotation hypothesis holds, this curvature must be the result of deformation with a non-coaxial shearing component. In the PBIS strain model coaxial deformation early in an event will not have partitioned at the scale of a porphyroblast (compare Fig. 2b with Fig. 2c). A growing porphyroblast will include the curvature of the foliation being crenulated, partitioning the more intense deformation around its rim as shearing intensifies. The strain does not appear to intensify towards the edges of the core part of the garnet. This observation is consistent with the suggestion by Bell and Hayward (1991) and Bell et al. (2004) that porphyroblasts only grow early in deformation. They argue that growth only occurs syn-deformation and stops once the crenulation cleavage has begun to differentiate (stage 3 of Bell & Rubenach 1983).

Under the non-rotational hypothesis the relative rotation of porphyroblast and foliation is implied. However, as Stallard et al. (2002) argue, the geometry of curved inclusion trails does not provide conclusive evidence as to the processes that form them. Both hypotheses can be used to explain the observed geometries; taken individually, the 3-D inclusion trail geometry of the cores of the porphyroblasts studied here cannot be used to argue for or against either model.

### 4.2.2 Core Foliation Data

The orientations of the poles to the core foliations show a moderately clustered distribution with a shallow westerly plunge. The centred stereonet in Fig. 9h shows that these data have a slight girdle component to its distribution with an axis plunging at 22.8° towards 194.9°, similar to the orientation of the core FIA. This suggests that there may be some rotation of the foliation about that FIA.

It is important to note the eigenvalue analysis shows that the data has a predominantly clustered distribution. If the porphyroblasts have not rotated, then the distribution observed must be attributed to a primary variation in the orientation of the foliation before porphyroblast growth. There is little literature on the amount of variation in the orientation of a single foliation. Many factors will influence this such as cleavage refraction, reactivation, intensity of the foliation and the anastomosing nature of foliations. Treagus (1983, 1988) demonstrated that cleavage orientation can vary markedly as the result of relatively small variations in the competency of rock. Variations in the mineralogy of the matrix are observed in sample V209 (Fig. 3); therefore, it is possible that cleavage refraction may be the cause of some the variation in the orientation of the foliation. Bell (1978`; Fig. 22) measured the preferred orientation of micas in a slaty cleavage and found distributions similar to those observed here for the core foliation. He attributed this to the anastomosing nature of foliations. It can be concluded that the distribution observed in the orientations of the foliation measured in the cores of the porphyroblasts is consistent with the variation being a primary feature of the rock that has not been modified by subsequent foliation forming events. The slight girdle distribution of these data about the FIA observed in Fig. 9h is consistent with the interpretation that the growth of the garnet cores occurred early in the same deformation that resulted in strong partitioning and development of a new foliation. The amount of rotation is small and the variation is dependent on the amount the foliation had rotated before individual porphyroblasts nucleated. This may also explain why these data do not fit a Watson bipolar distribution to an acceptable level of confidence.

If the rotational hypothesis was correct, a shape parameter (Woodcock 1977) no greater than two would be expected but the foliation data has a shape parameter of 3.9. Drill Core 3 has a shape parameter of only 1.68 with a $t_1$ axis that is approximately the same as the core FIA. This is most likely a result of the small sample size as the variation in FIA dip in the drill core is

only 40º, which is less than that for the total sample population. For the rotation hypothesis to hold, all porphyroblasts must have rotated by similar amounts to each other. The volume of garnet in this sample is such that it is highly unlikely that there would be no interaction between them. Garnets "colliding" should either act as one and rotate together or act like interconnecting cogs driving one another in opposite directions. It is difficult to imagine a clustered distribution if rotation had been the case, because of the range of possible rotation rates, as pointed out by Beirmier and Stüwe (2003), who showed that interaction between porphyroblasts could result in rotation rates between 25% and 75% of the shear strain rate using numerical models. The radius of garnet porphyroblasts varies from 1mm to over 3mm yet they have a consistent foliation orientation. This is problematic if the garnet sizes are related to either the relative timing of nucleation or termination of growth. If all the porphyroblasts nucleate at the same point in time, continue to grow for the same time period, are all subject to the same shear strain rate, and all display the same relationship between shear strain rate and rotation rate, then the total amount of rotation will be the same for each of them and the preserved foliation would maintain a consistent orientation. This requires a set of circumstances that are considered highly improbable. For example, there have been several papers written that demonstrate that the size of garnet porphyroblasts correlate with timing of nucleation (e.g. Chernoff & Carlson 1997, Spear & Daniel 2003), while others give an example of a complicated growth history (Beirmeier & Stuwe 2003).

### 4.2.3 Core FIA Data

The core FIA data has a moderately clustered distribution, similar to that of the core foliation data. Comparing the centred steronet (8b) with that of the foliation data (8h) the tighter cluster is readily observed. A slightly skewed distribution is observed (see also Fig.11a). However, this does not appear significant and these data are well represented by a Watson bipolar model, suggesting that the slightly skewed nature is the result of sampling error. There is no suggestion of a girdle component to the distribution. The 95% confidence cone has a semiangle of only 4.15º.

According to Bell et al. (1995), FIAs are equivalent to the intersection axis between two foliations. If the non-rotation model is correct some conclusions about these foliations can be drawn. It was not possible to directly measure the second, crenulating foliation in any of the porphyroblasts because only the curvature into it is preserved. There are also complications that result from the influence of the porphyroblast shape. It is impossible to derive the orientation of the crenulating foliation from the FIA and core foliation data alone because there are many solutions to this problem (Fig. 12a). However, the most likely orientation for the crenulating foliation in this is a sub-horizontal foliation with a southerly dip, as demonstrated in Fig. 12.

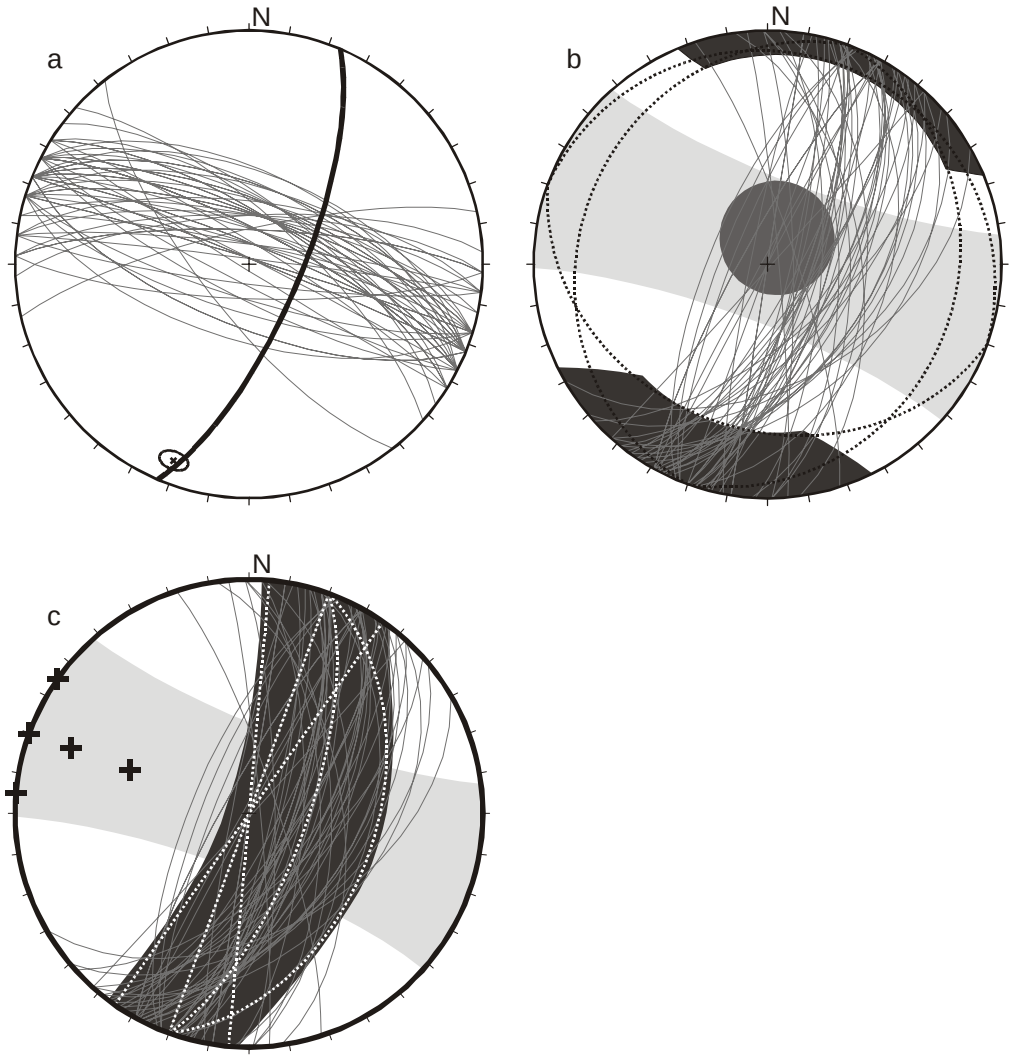


**Figure 12.** A series of equal area stereonets demonstrating that the core FIA is most likely the result of the crenulation of a steep foliation by a sub-horizontal one. (a) shows the mean FIA and 95% confidence interval (cross and circle), the mean core foliation (heavy black line) and the great circles perpendicular to the 58 FIA measurements (light grey lines). The pole to the foliation intersecting with the steep core foliation to form the FIAs must lie on this great circle for each FIA, so the mean orientation must lie in the light grey areas of (b) and (c). In (b) the crenulating foliation is taken to be sub-horizontal with a mean dip and dip-direction of 10° → 200° with a 20° spread (poles would plot in mid-grey circle). The possible intersections between this (dotted lines) and the steep core foliation (light grey lines) are shown in dark grey. Note that this distribution closely matches that for the actual FIA measurements. In (c), the crenulating foliation (dotted lines with + marking the poles) has a moderate to steep dip as in. The range of possible intersections has a much greater spread so is considered an unlikely scenario.

The alignment of zones of maximum curvature of the inclusion trails in the core part of porphyroblasts supports this conclusion.

When introducing the concept of FIAs, Hayward (1990) argued that they would generally have a shallow plunge. This was based on the observation of alternating near-vertical and near horizontal foliations by Bell and Johnson (1989) who proposed a orogenic model involving cycles of horizontal compression and gravitational collapse. The data presented here is in agreement with this idea, and other published data (see Bell et al. 1992c and references

therein). An important implication of this model is that the FIA orientation represents the strike of the sub-vertical foliation. When looking for correlations between the FIAs and sub-vertical core foliation preserved in the porphyroblasts, the only correlation found is between their 2-D trends. There was no statistically significant correlation between the spherical datasets. This means that the dip of the foliation has little to do with the orientation of the FIAs and that they do indeed reflect the strike of the steep foliation.

If a rotational model applies, the FIA is the rotation axis about which the porphyroblasts rotate as they include a single foliation. It is not possible to draw any conclusions about the orientation of this foliation if it is not preserved in the matrix. The effects of subsequent deformation events also need to be considered.

As mentioned above the FIAs appear to be curvilinear, a result of the progressive nature of deformation. A process by which this would occur in the non-rotational model is shown in Fig. 34 of Bell et al. (1986). As deformation progresses the crenulation hinge is rotated towards the orientation of the stretching lineation of the deformation event that the porphyroblast has grown in, resulting in asymmetrical curvature of the FIA in the plane of the later foliation. This is the same as the concept as that for doubly plunging folds that form as a result of heterogeneous strain. In a rotational model, a shift in the stretching direction would be required, or a rotation of the foliation relative to the porphyroblast.

The orientation of the core FIA, as measured here, differs by 24º from that reported by Bell et al. (1998). They used the asymmetry method to determine the FIAs and did not have sections cut at 010º and 020º. The discrepancy results from sampling error in the selection of porphyroblasts within a section. The garnet density in this sample is unusually high and it would not be a common approach to examine every porphyroblast when up to 130 are present in each section. Bell et al. (1998) started with sections cut at 30º increments. They incorrectly determined that the FIA lay between the 030º and 060º, although this overlaps the distribution of FIAs measured by HRXCT. Appendix 1 lists the asymmetry observations for all garnets in all sections cut for this sample. The 030º section contains roughly the same number of garnets with each asymmetry. If the garnets sampled had predominantly clockwise trails one could easily come to an erroneous conclusion about the location of the FIA. A similar error could have been made with the 040º section. This suggests that care must be taken to record the asymmetry in all porphyroblasts in a thin section when applying the asymmetry method, particularly in sections containing trails with both asymmetries. The median FIA value reported by Bell et al. (1998) correlates well with that reported here.

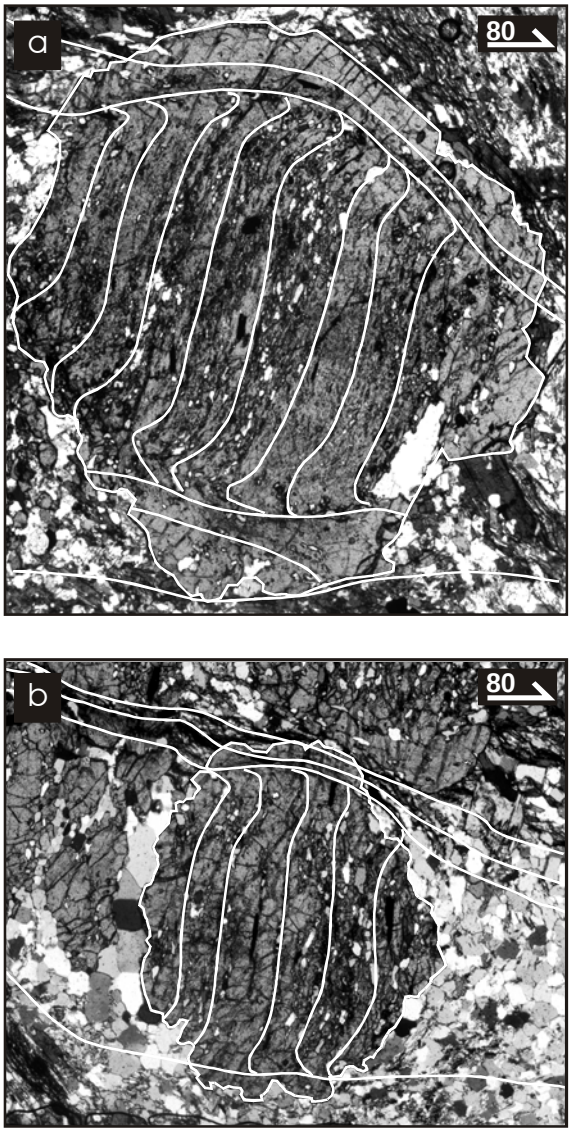


**Figure 13.** Photomicrographs from a vertical thin section of sample V209 showing the history preserved in the inclusion trails. Both show the steep trails in the core of the garnet that curves in a top to the east sense. This is interpreted as S1 being crenulated by a sub-horizontal S2. S2 then curves into S3 which is only preserved in a small part radial increment of garnet. S3 is interpreted as being sub-vertical, and is more pronounced in the upper part of the garnet in (b). S3 then curves into S4, a sub-horizontal foliation that is preserved in the rim of the garnets. Bottom edge of both images is approximately 4.5mm.

### 4.2.4 Variation Between Drill Cores

Statistical tests show that all four drill cores sample the same population for both the FIAs and core foliations. The variations seen in the mean orientations are simply a reflection of the low number of observations from each drill core. There is no evidence of a pre-existing folding of the core foliation. It is possible that if more measurements were made at the locations of each of the drill cores the variation in mean orientations would prove significant. This would be due to the anastomosing nature of foliations and would be the case in either the rotation or the non-rotation models.

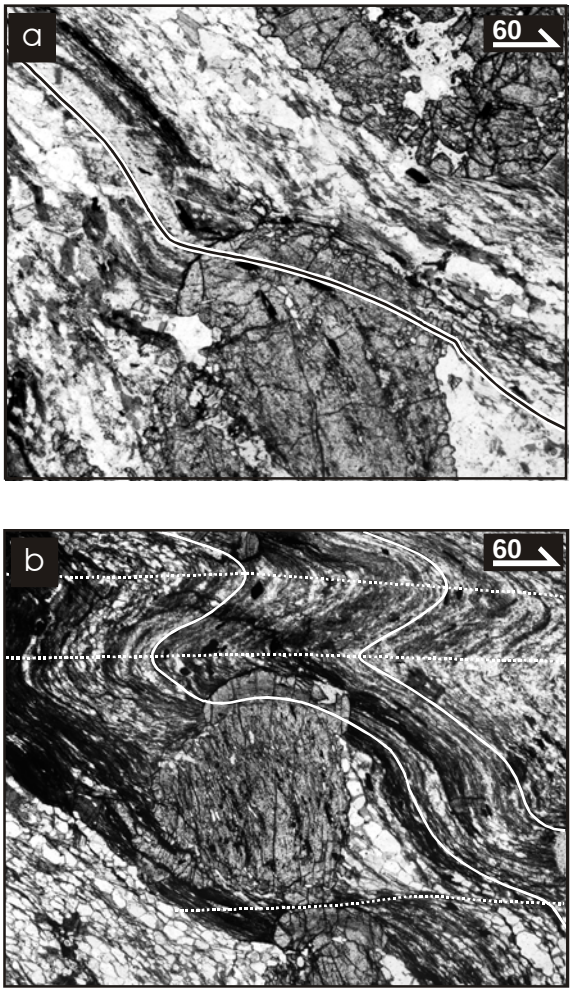


**Figure 14.** Photomicrographs from a vertical thin section of sample V209 showing the S4 to S5 transition in (a) and the S4 to S5 (solid lines) to S6 (dotted lines) transitions in (b). The garnets in both images have been cut close to their rim so the trails do not show the full history. Bottom edge of (a) is approximately 4.5mm and of (b) is 6mm.

### 4.2.5 Median FIA Data

Although the number of observations is low (n=17) the median FIA appear to be sampling an even tighter distribution. Bell and Johnson (1989) argued that as strain is concentrated against rigid bodies such as porphyroblasts it will more closely reflect the direction of bulk shortening. This would result in a more tightly clustered distribution of FIAs that form in growth increments on pre-existing porphyroblasts in the non-rotation model. The plunge of the median FIA could not be measured. It is most likely horizontal as curvature attributed to this event is restricted to the top and bottoms of the porphyroblasts. In the rotational model, the tighter distribution of a later FIA event would be expected as earlier FIA would have been subjected to more deformation events.

## *4.3 Evidence for Non-rotation and a Prolonged History*

Does the evidence support a rotation or non-rotation hypothesis? The clustering of the FIA and foliation data for the core provides compelling evidence that the porphyroblasts in this

sample have not rotated. The clustering of the core foliation data is difficult to reconcile with the rotation hypothesis because a more girdle like distribution about the roatation axis would be expected from rotation in a single foliation forming event. The Woodcock shape parameter (K) for the foliation data is 3.9; it would be expected to be less than two if the porphyroblasts had rotated. Subsequent foliation forming events would create a dispersed distribution. The median FIA is roughly orthogonal to the core FIA. In the rotation hypothesis, this would indicate a second rotation about an axis perpendicular to the first, yet there is no evidence that the core FIAs have been redistributed in such a way. A girdle distribution about the median FIA would be expected. As well as the foliation forming events that formed the core and median foliations, there is evidence for at least three more foliations in the sample (Fig. 14). Again, there is no evidence that the deformation events forming these foliations have affected the distribution of the earlier structures preserved in the porphyroblasts. As mentioned above, the distribution of data observed here is best explained by the variation of the primary fabrics without any rotation with respect to a fixed geographic reference frame.

If rotation had occurred, all the porphyroblasts would have to have rotated by approximately the same amount as each other in each deformation event. This is considered implausible given the garnet density and the interference that would result (Beirmeier & Stuwe 2003). Another hypothesis is that the porphyroblasts did rotate as the garnet cores grew but not in latter deformation events. This would require that all the porphyroblasts rotated in a remarkably consistent manner in the foliation-forming event preserved in the garnet cores and for the deformation mechanism to change between deformation events. Both of these conditions are highly improbable. It is important to note that the rotation and non-rotation hypotheses for the formation of curved inclusion trails are mutually exclusive in the one foliation-forming event because they require opposite shear senses (see Fig.1); curvature cannot form by a combination of the two. If there were a switch from a rotation to a non-rotation process a reversal in the asymmetry of the inclusion trails would be expected.

As the porphyroblasts have not rotated the structures preserved within them can be used to determine the early deformation history preserved in this sample (Figs. 13 and 14). Garnet nucleated and grew during the early stages of the development of a sub-horizontal foliation ($S_2$) that was crenulating a steeply east dipping foliation ($S_1$). The porphyroblasts preserved the curvature of $S_1$ towards $S_2$ as they grew early in $D_2$ before significant differentiation had occurred (Fig. 13). The core FIA preserves the orientation of the intersection between these two foliations ($L_2^1$). The shear sense on $S_2$ was top to the east. A sub-vertical 110º striking crenulation cleavage with a south side down shear sense then developed ($S_3$). The curvature of $S_2$ into $S_3$ was captured in a small radial increment of garnet growth and is preserved as the median FIA (equivalent to $L_3^2$, Fig 13). This growth could have occurred early in $D_3$, $D_4$ or

both. Another sub-horizontal foliation then formed ($S_4$) which is preserved in some of the porphyroblasts as a truncational surface. $L_4^3$ would have approximately the same orientation as $L_3^2$ and the median FIA. $S_3$ curves into $S_4$ with a top to the south shear sense on $S_4$. The dominant matrix foliation formed next ($S_5$) with a sub-vertical north-northeast strike and a west side up shear sense (Fig 14a). The curvature of $S_4$ into $S_5$ is preserved in the rims of some of the porphyroblasts and the rim FIA is equivalent to $L_5^4$. The final deformation event formed a sub-horizontal foliation, $S_6$, that crenulates and folds $S_5$ in the matrix with a top to the west asymmetry (Figs 3 and 14b). Only $S_5$ and $S_6$ are preserved in the matrix and the earlier events can only be determined by studying the inclusion trail geometry. This demonstrates the value of curved inclusion trails of which Rosenfeld imagined.

# References


Aerden, D. 2004. Correlating deformation in Variscan NW-Iberia using porphyroblasts; implications for the Ibero-Armorican Arc. *Journal of Structural Geology* **26**(1), 177-196.

Aerden, D. 2005. Comment on Reference frame, angular momentum, and porphyroblast rotation by Dazhi Jiang and Paul F. Williams. *Journal of Structural Geology*, In Press.

Aerden, D. G. A. M. 1995. Porphyroblast non-rotation during crustal extension in the Variscan Lys-Caillaouas Massif, Pyrenees. *Journal of Structural Geology* **17**, 709-725.

Bauer, R. L., Ketcham, R. A., Dennison, C. & Carlson, W. D. 1998. X-ray computed tomography (CT) imaging of spiral inclusion trails and the external morphology of garnet porphyroblasts. *EOS* **79**(17), 357.

Beirmeier, C. & Stuwe, K. 2003. Strain rates from snowball garnet. *Journal of Metamorphic Geology* **21**, 253-268.

Bell, T. H. 1978. The development of slaty cleavage across the Nackara Arc of the Adelaide Geosyncline. *Tectonophysics* **51**(3-4), 171-174.

Bell, T. H. 1981. Foliation development -- The contribution, geometry and significance of progressive, bulk, inhomogeneous shortening. *Tectonophysics* **75**(3-4), 273-296.

Bell, T. H. 1985. Deformation partitioning and porphyroblast rotation in metamorphic rocks: a radical reinterpretation. *Journal of Metamorphic Geology* **3**, 109-118.

Bell, T. H. & Chen, A. 2002. The development of spiral-shaped inclusion trails during multiple metamorphism and folding. *Journal of Metamorphic Geology* **20**(4), 397 -412.

Bell, T. H., Duncan, A. C. & Simmons, J. V. 1989. Deformation partitioning, shear zone development and the role of undeformable objects. *Tectonophysics* **158**(1-4), 163-171.

Bell, T. H., Forde, A. & Hayward, N. 1992a. Do smoothly-curving spiral shaped inclusion trails signify porphyroblast rotation? *Geology* **20**, 59-62.

Bell, T. H., Forde, A. & Hayward, N. 1992b. Do smoothly curved, spiral-shaped inclusion trails signify porphyroblast rotation?: Reply. *Geology* **20**(11), 1055-1056.

Bell, T. H., Forde, A. & Wang, J. 1995. A new indicator of movement direction during orogenesis: measurement technique and application to the Alps. *Terra Nova* **V. 7**, 500-508.

Bell, T. H., Ham, A. P. & Hickey, K. A. 2003. Early formed regional antiforms and synforms that fold younger matrix schistosities: their effect on sites of mineral growth. *Tectonophysics* **367**(3-4), 253 -278.

Bell, T. H., Ham, A. P. & Kim, H. S. 2004. Partitioning of deformation along an orogen and its effects on porphyroblast growth during orogenesis. *Journal of Structural Geology* **26**(5), 825 -845.

Bell, T. H. & Hayward, N. 1991. Episodic metamorphic reactions during orogenesis; the control of deformation partitioning on reaction sites and reaction duration. *Journal of Metamorphic Geology* **9**(5), 619-640.

Bell, T. H. & Hickey, K. A. 1997. Distribution of pre-folding linear indicators of movement direction around the Spring Hill Synform, Vermont; significance for mechanism of folding in this portion of the Appalachians. *Tectonophysics* **274**(4), 275-294.

Bell, T. H. & Hickey, K. A. 1999. Complex microstructures preserved in rocks with a simple matrix; significance for deformation and metamorphic processes. *Journal of Metamorphic Geology* **17**(5), 521-535.

Bell, T. H., Hickey, K. A. & Upton, G. J. G. 1998. Distinguishing and correlating multiple phases of metamorphism across a multiply deformed region using the axes of spiral, staircase and sigmoidal inclusion trails in garnet. *Journal of Metamorphic Geology* **16**(6), 767-794.

Bell, T. H., Hickey, K. A. & Wang, J. 1997. Spiral and staircase inclusion trail axes within garnet and staurolite porphyroblasts from schists of the Bolton Syncline, Connecticut; timing of porphyroblast growth and the effects of fold development. *Journal of Metamorphic Geology* **15**(4), 467-478.

Bell, T. H. & Johnson, S. E. 1989. Porphyroblast inclusion trails: the key to orogenesis. *Journal of Metamorphic Geology* **7**, 279-310.

Bell, T. H. & Johnson, S. E. 1990. Rotation of relatively large rigid objects during ductile deformation: Well established fact or intuitive prejudice. *Australian Journal of Earth Sciences* **37**, 441-446.

Bell, T. H., Johnson, S. E., Davis, B., Forde, A., Hayward, N. & Witkins, C. 1992c. Porphyroblast inclusion-trail orientation data; eppure non son girate! *Journal of Metamorphic Geology* **10**(3), 295-307.

Bell, T. H. & Mares, V. M. 1999. Correlating deformation and metamorphism around orogenic arcs. *American Mineralogist* **84**(11-12), 1727 -1740.

Bell, T. H. & Rubenach, M. J. 1983. Sequential porphyroblast growth and crenulation cleavage development during progressive deformation. *Tectonophysics* **92**(1-3), 171-194.

Bell, T. H., Rubenach, M. J. & Fleming, P. D. 1986. Porphyroblast nucleation, growth and dissolution in regional metamorphic rocks as a function of deformation partitioning during foliation development. *Journal of Metamorphic Geology* **4**, 37-67.

Bell, T. H. & Welch, P. W. 2002. Prolonged Acadian orogenesis: Revelations from foliation intersection axis (FIA) controlled monazite dating of foliations in porphyroblasts and matrix. *American Journal of Science* **302**(7), 549 -581.

Berger, M. J., Hubbell, J. H., Seltzer, S. M., Coursey, J. S. & Zucker, D. S. 1999. XCOM: Photon Cross Section Database (version 1.2), [Online]. **2002**. National Institute of Standards and Technology, Gaithersburg, MD.

Bonse, U. & Beckmann, F. 2001. Multiple-beam X-ray interferometry for phase-contrast microtomography. *Journal of Synchrotron Radiation* **8**(Part 1), 1-5.

Bonse, U. & Busch, F. 1996. X-ray computed microtomography (μCT) using synchrotron radiation (SR). *Progress in biophysics and molecular biology* **65**, 133-169.

Bronnikov, A. V. 2002. Theory of quantitative phase-contrast computed tomography. *Journal of the Optical Society of America A-Optics & Image Science* **19**(3), 472-480.

Carlson, W. D. & Denison, C. 1992. Mechanisms of porphyroblast crystallization; results from high-resolution computed X-ray tomography. *Science* **257**(5074), 1236-1239.

Ceriani, S., Mancktelow, N. S. & Pennacchioni, G. 2003. Analogue modelling of the influence of shape and particle/matrix interface lubrication on the rotational behaviour of rigid particles in simple shear. *Journal of Structural Geology* **25**(12), 2005-2021.

Chernoff, C. B. & Carlson, W. 1997. Disequilibrium for Ca during growth of pelitic garnet. *Journal of Metamorphic Geology* **15**(4), 421-438.

Chernoff, C. B. & Carlson, W. 1999. Trace element zoning as a record of chemical disequilibrium during garnet growth. *Geology* **27**(6), 555-558.

Cifelli, R. L., Rowe, T. B., Luckett, W. P., Banta, J., Reyes, R. & Howes, H. I. 1996. Fossil evidence for the origin of the marsupial pattern of tooth replacement. *Nature* **379**, 715-718.

Cihan, M. 2004. The drawbacks of sectioning rocks relative to fabric orientations in the matrix: A case study from the Robertson River Metamorphics (Northern Queensland, Australia). *Journal of Structural Geology* **26**, 2157 -2174.

Cihan, M. & Parsons, A. 2005. The use of porphyroblasts to resolve the history of macro-scale structures: an example from the Robertson River Metamorphics, North-Eastern Australia. *Journal of Structural Geology* **27**(6), 1027-1045.

Daniel, C. G. & Spear, F. S. 1998. Three-dimensional patterns of garnet nucleation and growth. *Geology* **v.26**, 503-506.

Daniel, C. G. & Spear, F. S. 1999. The clustered nucleation and growth processes of garnet in regional metamorphic rocks from north-west Connecticut, USA. *Journal of Metamorphic Geology* **17**(5), 503.

Davis, B. K. 1993. Mechanism of emplacement of the Cannibal Creek Granite with special reference to timing and deformation history of the aureole. *Tectonophysics* **224**, 337-362.

De Man, B., Nuyts, J., Dupont, P., Marchal, G. & Suetens, P. 2001. An iterative maximum-likelihood polychromatic algorithm for CT. *IEEE Transactions on Medical Imaging* **20**(10), 999-1008.

Denison, C., Carlson, W. D. & Ketcham, R. A. 1997. Three-dimensional quantitaitve textural analysis of metamorphic rocks using high-resolution computed X-ray tomography: Part I. Methods and techniques. *Journal of Metamorphic Geology* **15**(1), 29-44.

Dilmanian, F. A. 1992. Computed tomography with monochromatic X-rays. *American Journal of Physiological Imaging* **7**, 175-193.

Elbakri, I. A. & Fessler, J. A. 2003. Segmentation-free statistical image reconstruction for polyenergetic x-ray computed tomography with experimental validation. *Physics in Medicine & Biology* **48**(15), 2453-2477.

Evins, P. M. 2005. A 3D study of aligned porphyroblast inclusion trails across shear zones and folds. *Journal of Structural Geology* **27**(7), 1300-1314.

Fisher, N. I. 1993. *Statistical analysis of circular data*. Cambridge University Press, Cambridge, [England].

Fisher, N. I. & Lee, A. J. 1983. A correlation coefficient for circular data. *Biometrika* **70**(2), 327-332.

Fisher, N. I., Lewis, T. & Embleton, B. J. J. 1987. *Statistical analysis of spherical data*. Cambridge University Press, Cambridge [England] ; Melbourne.

Ham, A. P. & Bell, T. H. 2004. Recycling of foliations during folding. *Journal of Structural Geology* **26**(11), 1989-2009.

Hayward, N. 1990. Determination of early fold axis orientations in multiply deformed rocks using porphyroblast inclusion trails. *Tectonophysics* **V. 179**, 353-369.

Hayward, N. 1992. Microstructural analysis of the classical spiral garnet porphyroblasts of South-east Vermont; evidence for non-rotation. *Journal of Metamorphic Geology* **10**(4), 567-587.

Hickey, K. A. & Bell, T. H. 1999. Behaviour of rigid objects during deformation and metamorphism; a test using schists from the Bolton Syncline, Connecticut, USA. *Journal of Metamorphic Geology* **17**(2), 211-228.

Hobbs, B. E., Means, W. D. & Williams, P. F. 1976. *An Outline of Structural Geology*. John Wiley and Sons, New York.

Huddlestone-Holmes, C. R. & Ketcham, R. A. 2005. Getting the inside story: using computed X-ray tomography to study inclusion trails in garnet porphyroblasts. *American Mineralogist* **90**, ea1-ea17.

Ikeda, T., Shimobayashi, N., Wallis, S. R. & Tsuchiyama, A. 2002. Crystallographic orientation, chemical composition and three dimensional geometry pf sigmoidal garnet: evidence for rotation. *Journal of Structural Geology* **24**, 1633-1646.

Ilg, B. R. & Karlstrom, K. E. 2000. Porphyroblast inclusion trail geometries in the Grand Canyon: evidence for non-rotation and rotation? *Journal of Structural Geology* **22**, 231-243.

Johnson, S. E. 1990. Lack of porphyroblast rotation in the Otago schists, New Zealand: implications for crenulation cleavage development, folding and deformation partitioning. *Journal of Metamorphic Geology* **8**, 13-30.

Johnson, S. E. 1993a. Testing models for the development of spiral-shaped inclusion trails in garnet porphyroblasts: to rotate or not to rotate, that is the question. *Journal of Metamorphic Geology* **11**, 635-659.

Johnson, S. E. 1993b. Unravelling the spirals: a serial thin-section study and three dimensional computer-aided reconstruction of spiral-shaped inclusion trails in garnet porphyroblasts. *Journal of Metamorphic Geology* **11**, 621-634.

Johnson, S. E. 1999. Porphyroblast microstructures: A review of current and future trends. *American Mineralogist* **V.84**, 1711-1726.

Johnson, S. E. & Moore, R. R. 1996. De-bugging the 'millipede' porphyroblast microstructure: a serial thin-section study and 3-D computer animation. *Journal of Metamorphic Geology* **14**, 3-14.

Jones, K. W., Feng, H., Lindquist, W. B., Adler, P. M., Thovert, J. F., Vekemans, B., Vincze, L., Szaloki, I., Van Grieken, R., Adams, F. & Riekel, C. 2003. Study of the microgeometry of porous materials using synchrotron computed microtomography. In: *Applications of X-Ray Computed Tomography in the Geosciences* (edited by Mees, F., Swennen, R., Van Geet, M. & Jacobs, P.). *Geological Society Special Publication (215)* **215**. Geological Society of London, London, 39-49.

Jung, W. S., Ree, J. H. & Park, Y. 1999. Non-rotation of garnet porphyroblasts and 3-D inclusion trail data: an example from the Imjingang belt, South Korea. *Tectonophysics* **307**(3-4), 381-395.

Kak, A. C. & Slaney, M. 1988. *Principles of Computerized Tomographic Imaging*. The Institute of Electrical and Electronics Engineers, Inc., New York.

Kalukin, A. R., Van Geet, M. & Swennen, R. 2000. Principal components analysis of multienergy X-ray computed tomography of mineral samples. *IEEE Transactions on Nuclear Science* **47**(5), 1729-1736.

Ketcham, R. A. 2004. Efficient and flexible three-dimensional measurement of features in CT data volumes: implications for quantitative analysis of metamorphic textures. In: *32nd International Geological Congress* **Abstract Volume, Part 1**, Florence, Italy, Abstract 93-4, 445.

Ketcham, R. A. & Carlson, W. D. 2001. Acquisition, optimization and interpretation of X-ray computed tomographic imagery: applications to the geosciences. *Computers and Geosciences* **27**, 381-400.

Ketcham, R. A. & Ryan, T. 2004. Quantification and visualization of anisotropy in trabecular bone. *Journal of Microscopy* **213**, 158-171.

Koeberl, C., Denison, C., Ketcham, R. A. & Reimold, W. U. 2002. High resolution X-ray computed tomography of impactites. *Journal of Geophysical Research - Planets* **107(E10)**, 5089.

Krukowski, S. T. 1988. Sodium metatungstate: a new heavy-mineral separation medium for the extraction of conodonts from insoluble residues. *Journal of Paleontology* **62**(2), 314-316.

Kyle, J. R. & Ketcham, R. A. 2003. In-situ distribution of gold in ores using high-resolution X-ray computed tomography. *Economic Geology* **98**, 1697-1701.

Lee, H., Lee, B.-J. & Otoh, S. 2000. Significance of systematic changes in crenulation asymmetries within meta-sediments across the Ogcheon Supergroup in the Goesan area, southern Korea. Hanrimwon Publishing Company for the Geological Society of Korea, Seoul, South Korea, 115-134.

Lister, G. S. & Williams, P. F. 1983. The partitioning of deformation in flowing rock masses. *Tectonophysics* **92**, 1-33.

Mancktelow, N. S., Arbaret, L. & Pennacchioni, G. 2002. Experimental observations on the effect of interface slip on rotation and stabilisation of rigid particles in simple shear and a comparison with natural mylonites. *Journal of Structural Geology* **24**(3), 567-585.

Marschallinger, R. 1998. Three-dimensional reconstruction and modelling of microstructures and microchemistry in geological materials. *Scanning* **20**, 65-73.

Masuda, T. & Mochizuki, S. 1989. Development of snowball structure: numerical simulation of inclusion trails during synkinematic porphyroblast growth in metamorphic rocks. *Tectonophysics* **170**, 141-150.

Mees, F., Swennen, R., van Geet, M. & Jacobs, P. 2003. *Applications of X-ray computed tomography in the geosciences*. Geological Society of London, London.

Natterer, F. & Ritman, E. L. 2002. Past and Future Directions in X-Ray Computed Tomography (CT). *International Journal of Imaging Systems and Technology* **12**, 175-187.

Passchier, C. W. & Trouw, R. A. J. 1996. *Microtectonics*. Springer-Verlag, Berlin.

Passchier, C. W., Trouw, R. A. J., Zwart, H. J. & Vissers, R. L. M. 1992. Porphyroblast rotation: eppur si muove? *Journal of Metamorphic Geology* **10**, 283-294.

Powell, D. & Treagus, J. E. 1967. On the geometry of S-shaped inclusion trails in garnet porphyroblasts. *Mineralogical Magazine* **36**, 453-456.

Powell, D. & Treagus, J. E. 1970. Rotational fabrics in metamorphic minerals. *Mineralogical Magazine* **37**(No. 291), 801-813.

Proussevitch, A., Ketcham, R. A., Carlson, W. & Sahagian, D. 1998. Preliminary results of X-ray CT analysis of Hawaiian vesicular basalts. In: *American Geophysical Union 1998 spring meeting* (edited by Anonymous) **79**. American Geophysical Union, 360.

Ramsay, J. G. 1962. The geometry and mechanics of formation of 'similar' type folds. *Journal of Geology* **70**, 309-327.

Rosenfeld, J. 1968. Garnet rotations due to the major paleozoic deformations in southeast Vermont. In: *Studies of Appalachian Geology: Northern and Maritime* (edited by Zen, E., White, W. S., Hadley, J. B. & Thompson, J., J.B.). Wiley-Interscience Publishers, New York, 185 - 202.

Rosenfeld, J. L. 1970. *Rotated Garnets in Metamorphic Rocks. Geological Society of America Special Paper, 129*. Geological Society of America, Boulder, Colarado.

Rowe, T. 1996. Coevolution of the mammalian middle ear and neocortex. *Science* **273**, 651-654.

Samanta, S. K., Mandal, N. & Chakraborty, C. 2002a. Development of structures under the influence of heterogeneous flow field around rigid inclusions: insights from theoretical and numerical models. *Earth-Science Reviews* **58**(1-2), 85-119.

Samanta, S. K., Mandal, N., Chakraboty, C. & Majumder, K. 2002b. Simulation of inclusion trail patterns within rotating synkinematic porphyroblasts. *Computers and Geosciences* **28**, 297-308.

Sayab, M. 2005. Microstructural evidence for N-S shortening in the Mount Isa Inlier (NW Queensland, Australia): the preservation of early W-E-trending foliations in porphyroblasts revealed by independent 3D measurement techniques. *Journal of Structural Geology* **27**(8), 1445-1468.

Schoneveld, C. 1977. A study of some typical inclusion patterns in strongly paracrystalline-rotated garnets. *Tectonophysics* **39**, 453-471.

Spear, F. & Yao, K. 2001. The three dimensional geometry of garnet growth, Harpswell Neck, Maine, USA. In: *Eleventh Annual V.M. Goldschmidt Conference, Hot Springs, VA, USA. Abstract number, 3693.* (edited by Bodnar, R. J. & Hochella, M. F.). Lunar and Planetary Institute, Houston, Texas.

Spear, F. S. & Daniel, C. G. 1998. Three-dimensional imaging of garnet porphyroblast sizes and chemical zoning: Nucleation and growth history in the garnet zone. *Geological Materials Research* **1**(1), 1-43.

Spear, F. S. & Daniel, C. G. 2001. Diffusion control of garnet growth, Harpswell Neck, Maine, USA. *Journal of Metamorphic Geology* **19**(2), 179.

Spear, F. S. & Daniel, C. G. 2003. Three-dimensional imaging of garnet porphyroblast sizes and chemical zoning; nucleation and growth history in the garnet zone. *American Mineralogist* **88**(1), 245.

Stallard, A. & Hickey, K. A. 2001. Shear zone vs folding for spiral inclusion trails in the Canton Schist. *Journal of Structural Geology* **23**, 1845-1864.

Stallard, A., Ikei, H. & Masuda, T. 2002. Numerical simulations of spiral-shaped inclusion trails: can 3D geometry distinguish between end-member models of spiral formation? *Journal of Metamorphic Geology* **20**, 801-812.

Steinhardt, C. 1989. Lack of porphyroblast rotation in noncoaxially deformed schists from Petrel Cove, South Australia, and its implications. *Tectonophysics* **158**, 127-140.

Stewart, L. K. 1997. Experimental investigation of the effects of fluid heterogeneity upon the motion of rigid ellipsoidal inclusions during bulk inhomogeneous shortening. *Journal of Structural Geology* **19**(9), 1231-1243.

Takeda, T., Momose, A., Yu, Q. W., Yuasa, T., Dilmanian, F. A., Akatsuka, T. & Itai, Y. 2000. New types of X-ray computed tomography (CT) with synchrotron radiation: Fluorescent X-ray CT and phase-contrast X-ray CT using interferometer. *Cellular & Molecular Biology* **46**(6), 1077-1088.

ten Grotenhuis, S. M., Passchier, C. W. & Bons, P. D. 2002. The influence of strain localisation on the rotation behaviour of rigid objects in experimental shear zones. *Journal of Structural Geology* **24**(3), 485-499.

Timms, N. E. 2003. Garnet porphyroblast timing and behaviour during fold evolution: implications from a 3-D geometric analysis of a hand-sample scale fold in a schist. *Journal of Metamorphic Geology* **21**(9), 853-873.

Torikoshi, M., Tsunoo, T., Endo, M., Noda, K., Kumada, M., Yamada, S., Soga, F. & Hyodo, K. 2001. Design of synchrotron light source and its beamline dedicated to dual-energy x-ray computed tomography. *Journal of Biomedical Optics* **6**(3), 371-377.

Torikoshi, M., Tsunoo, T., Sasaki, M., Endo, M., Noda, Y., Ohno, Y., Kohno, T., Hyodo, K., Uesugi, K. & Yagi, N. 2003. Electron density measurement with dual-energy x-ray CT using synchrotron radiation. *Physics in Medicine & Biology* **48**(5), 673-685.

Treagus, S. H. 1983. A new theory of finite strain variation through contrasting layers, and its bearing on cleavage refraction. *Journal of Structural Geology* **5**, 351-358.

Treagus, S. H. 1988. Strain refraction in layered systems. *Journal of Structural Geology* **10**(5), 517-527.

Tsuchiyama, A., Nakamura, T., Nakano, T. & Nakamura, N. 2002. Three-dimensional description of the Kobe meteorite by micro X-ray CT method: Possibility of three-dimensional curation of meteorite samples. *Geochemical Journal* **36**, 369-390.

Upton, G. J. G. & Fingleton, B. 1989. *Spatial Data Anlysis by Example, Volume 2: Categorical and Directional Data*. John Wiley & Sons, Chichester.

Upton, G. J. G., Hickey, K. A. & Stallard, A. 2003. Regression models for cyclic data. *Royal Statistical Society* **Journal. Series C: Applied Statistics. 52**(Part 2), 227-235.

Wellington, S. L. & Vinegar, H. J. 1987. X-ray computerized tomography. *Journal of Petroleum Technology*(August 1987), 885-898.

Williams, P. F. & Jiang, D. 1999. Rotating garnets. *Journal of Metamorphic Geology* **17**, 367-378.

Woodcock, N. H. 1977. Specification of fabric shapes using an eigenvalue method. *Geological Society of America Bulletin* **88**, 1231-1236.

Woodcock, N. H. & Naylor, M. A. 1983. Randomness testing in three-dimensional orientation data. *Journal of Structural Geology* **5**(5), 539-548.

Yamaya, T., Obi, T., Yamaguchi, M. & Ohyama, N. 2000. An acceleration algorithm for image reconstruction based on continuous-discrete mapping model. *Optical Review* **7**(2), 132-137.

Yeh, M.-W. & Bell, T. H. 2004. Significance of dextral reactivation of an E-W transfer fault in the formation of the Pennsylvania orocline, central Appalachians. *Tectonics* **23**, TC5009, doi:10.1029/2003TC001593.

# Appendix 1. V209 Asymmestry Data.

**Asymmetry observations from thin sections, sample V209.**

| | | *Core* | | | | *Median* | | | | |
|---|---|---|---|---|---|---|---|---|---|---|
| Orientaion* | Rim Cut | cw | acw | millipede | amb.[#] | cw | acw | millipede | amb.[#] | Total |
| 000 | 24 | 41 | 2 | 0 | 3 | 43 | 0 | 0 | 3 | 70 |
| 010 | 33 | 46 | 13 | 0 | 39 | 54 | 0 | 0 | 44 | 131 |
| 020 | 35 | 34 | 28 | 4 | 4 | 51 | 0 | 0 | 19 | 105 |
| 030 | 31 | 11 | 12 | 1 | 7 | 23 | 0 | 0 | 8 | 62 |
| 040 | 27 | 5 | 17 | 2 | 11 | 20 | 0 | 0 | 15 | 62 |
| 050 | 50 | 4 | 24 | 1 | 21 | 26 | 0 | 0 | 24 | 100 |
| 060 | 39 | 1 | 52 | 0 | 15 | 47 | 0 | 0 | 21 | 107 |
| 070 | 16 | 0 | 25 | 0 | 1 | 23 | 0 | 0 | 3 | 42 |
| 080 | 34 | 0 | 42 | 0 | 6 | 39 | 0 | 0 | 9 | 82 |
| 090 | 38 | 0 | 49 | 0 | 5 | 40 | 6 | 1 | 7 | 92 |
| 100 | 28 | 0 | 55 | 0 | 1 | 34 | 13 | 3 | 6 | 84 |
| 110 | 25 | 0 | 43 | 0 | 5 | 23 | 16 | 3 | 6 | 73 |
| 120 | 25 | 0 | 50 | 0 | 1 | 20 | 21 | 4 | 6 | 76 |
| 130 | 41 | 0 | 41 | 1 | 5 | 8 | 15 | 8 | 16 | 88 |
| 140 | 17 | 0 | 31 | 0 | 2 | 5 | 19 | 2 | 7 | 50 |
| 150 | 26 | 0 | 41 | 1 | 10 | 0 | 32 | 2 | 18 | 78 |
| 160 | 28 | 0 | 30 | 0 | 9 | 0 | 24 | 0 | 15 | 67 |
| 170 | 26 | 2 | 42 | 0 | 8 | 0 | 38 | 0 | 14 | 78 |

* all orientations are to the left i.e. ←
[#] amb. = ambiguous

# Appendix 2. FIAs from HRXCT.

**FIA Measurements from HRXCT data, Sample V209.**

| | | | Core FIA* | | Core Foliation (Pole) | | Median FIA* |
|---|---|---|---|---|---|---|---|
| Core | Garnet | Diameter | Plunge | Direction | Plunge | Direction | Trend |
| 1 | 3 | 2.0 | 32.5 | 202.5 | 16.2 | 289.0 | - |
| 1 | 4 | 1.6 | 22.5 | 207.5 | 0.0 | 279.0 | - |
| 1 | 5 | 1.8 | 32.5 | 207.5 | 13.5 | 290.9 | - |
| 1 | 6 | 1.8 | 2.5 | 32.5 | 2.7 | 119.0 | 122.5 |
| 1 | 8 | 1.5 | 27.5 | 202.5 | 16.1 | 112.7 | - |
| 1 | 11 | 1.8 | 22.5 | 217.5 | 15.6 | 306.6 | - |
| 1 | 13 | 1.8 | 12.5 | 202.5 | 10.5 | 299.3 | - |
| 1 | 16 | 1.7 | 22.5 | 187.5 | 21.7 | 285.1 | 107.5 |
| 1 | 17 | 1.7 | 17.5 | 207.5 | 17.8 | 303.0 | 117.5 |
| 1 | 18 | 1.6 | 7.5 | 27.5 | - | - | - |
| 1 | 19 | 1.7 | 17.5 | 182.5 | 9.1 | 269.4 | - |
| 1 | 20 | 2.0 | 27.5 | 17.5 | 11.0 | 285.7 | - |
| 1 | 21 | 1.7 | 12.5 | 197.5 | 28.6 | 295.4 | 117.5 |
| 1 | 23 | 1.6 | 2.5 | 187.5 | 19.7 | 273.3 | 107.5 |
| 1 | 24 | 1.7 | 22.5 | 197.5 | 13.1 | 290.2 | - |
| 1 | 25 | 1.5 | 17.5 | 207.5 | 0.0 | 298.0 | - |
| 1 | 26 | 2.1 | 7.5 | 187.5 | 0.0 | 279.0 | 122.5 |
| 1 | 27 | 1.7 | 22.5 | 22.5 | 12.0 | 113.0 | - |
| 1 | 28 | 1.6 | 17.5 | 197.5 | 0.3 | 111.0 | - |
| 1 | 29 | 1.7 | 2.5 | 197.5 | 15.2 | 288.0 | - |
| 1 | 30 | 2.0 | 17.5 | 212.5 | 20.7 | 113.3 | - |
| 1 | 31 | 1.6 | 17.5 | 212.5 | 9.7 | 119.7 | - |
| 1 | 35 | 1.5 | 7.5 | 192.5 | 24.6 | 299.5 | - |
| 1 | 38 | 1 | 12.5 | 207.5 | - | - | - |
| 2 | 2 | 2.0 | 12.5 | 27.5 | 23.2 | 289.9 | 122.5 |
| 2 | 3 | 1.7 | 17.5 | 187.5 | 43.5 | 288.8 | - |
| 2 | 5 | 1.9 | 27.5 | 202.5 | 41.3 | 320.4 | 112.5 |
| 2 | 6 | 2.1 | 27.5 | 207.5 | 37.6 | 302.5 | - |
| 2 | 8 | 1.8 | 22.5 | 202.5 | 21.7 | 288.3 | - |
| 2 | 9 | 2.0 | 12.5 | 207.5 | 29.7 | 297.5 | - |
| 2 | 10 | 1.6 | 27.5 | 197.5 | 47.0 | 312.3 | - |
| 2 | 11 | 1.7 | 22.5 | 202.5 | 25.6 | 309.9 | 112.5 |
| 2 | 12 | 1.4 | 7.5 | 202.5 | 25.5 | 318.4 | |
| 2 | 14 | 1.7 | 2.5 | 202.5 | 24.5 | 298.5 | 112.5 |
| 2 | 16 | 1.5 | 12.5 | 207.5 | - | - | - |
| 3 | 1 | 1.7 | 7.5 | 212.5 | 37.9 | 304.3 | 127.5 |
| 3 | 3 | 2.0 | 17.5 | 52.5 | 42.3 | 330.0 | 122.5 |
| 3 | 6 | 1.5 | 17.5 | 197.5 | 38.1 | 306.2 | - |
| 3 | 7 | 2.6 | 17.5 | 192.5 | 40.1 | 309.3 | 117.5 |
| 3 | 8 | 2.0 | 17.5 | 202.5 | 29.3 | 312.0 | - |
| 3 | 9 | 2.1 | 17.5 | 202.5 | 22.0 | 307.6 | 117.5 |
| 3 | 11 | 1.7 | 22.5 | 212.5 | 16.6 | 304.2 | - |
| 3 | 12 | 1.7 | 17.5 | 222.5 | 1.6 | 312.0 | - |
| 4 | 1 | 1.7 | 12.5 | 167.5 | 10.7 | 252.9 | - |
| 4 | 2 | 1.7 | 2.5 | 202.5 | 15.1 | 290.7 | 117.5 |
| 4 | 4 | 1.9 | 17.5 | 177.5 | 33.6 | 262.6 | - |
| 4 | 5 | 2.1 | 22.5 | 22.5 | 15.4 | 296.1 | 112.5 |
| 4 | 7 | 1.0 | 12.5 | 17.5 | 4.3 | 265.2 | - |
| 4 | 8 | 1.6 | 17.5 | 17.5 | 9.8 | 119.7 | - |
| 4 | 9 | 1.7 | 7.5 | 7.5 | 35.4 | 274.1 | - |
| 4 | 11 | 1.7 | 2.5 | 207.5 | 6.9 | 101.7 | - |
| 4 | 12 | 1.9 | 7.5 | 202.5 | 31.5 | 297.2 | - |
| 4 | 13 | 1.0 | 12.5 | 182.5 | 10.9 | 282.9 | - |
| 4 | 15 | 2.1 | 12.5 | 207.5 | 26.8 | 298.7 | - |
| 4 | 16 | 1.8 | 7.5 | 197.5 | 8.7 | 284.8 | - |
| 4 | 18 | 1.7 | 12.5 | 2.5 | 29.7 | 269.1 | 117.5 |
| 4 | 24 | 1.9 | 2.5 | 197.5 | 18.7 | 286.9 | - |
| 4 | 25 | 1.6 | 12.5 | 182.5 | 25.0 | 269.5 | - |

*Middle value of 5° interval for which the data was measured.